Wide Transition-State Ensemble as Key Component for Enzyme Catalysis

Gabriel Ernesto Jara[1,4], Francesco Pontiggia[3,5], Renee Otten[3,6], Roman V. Agafonov[3,7], Marcelo A. Martí[2]* and Dorothee Kern [3]*

[1]Departamento de Química Inorgánica, Analítica y Química-Física (INQUIMAE-CONICET) and [2]Departamento de Química Biológica (IQUIBICEN-CONICET), Facultad de Ciencias Exactas y Naturales, Universidad de Buenos Aires, Buenos Aires, Argentina.

[3]Howard Hughes Medical Institute, Department of Biochemistry, Brandeis University, Waltham, Massachusetts, USA.

*Corresponding Author: Dorothee Kern (dkern@brandeis.edu); Marcelo A. Martí (marti.marcelo@gmail.com)

Current address: [4]Brazilian Biosciences National Laboratory (LNBio), Brazilian Center for Research in Energy and Materials (CNPEM), Campinas, SP, 13083-970, Brazil; [5] Psivant Therapeutics, Salem, MA, USA; [6] Treeline Biosciences, Watertown, MA, USA; [7] C4 Therapeutics, Watertown, MA, USA

Abstract

Transition-state theory has provided the theoretical framework to explain the enormous

rate accelerations of chemical reactions by enzymes. Given that proteins display large ensembles of conformations, unique transition states would pose a huge entropic bottleneck for enzyme catalysis. To shed light on this question, we studied the nature of the enzymatic transition state for the phosphoryl-transfer step in adenylate kinase by quantum-mechanics/molecular-mechanics calculations. We find a structurally wide set of energetically equivalent configurations that lie along the reaction coordinate and hence a broad transition-state ensemble (TSE). A conformationally delocalized ensemble, including asymmetric transition states, is rooted in the macroscopic nature of the enzyme. The computational results are buttressed by enzyme kinetics experiments that confirm the decrease of the entropy of activation predicted from such wide TSE. Transition-state ensembles as a key for efficient enzyme catalysis further boosts a unifying concept for protein folding and conformational transitions underlying protein function.

Introduction

Understanding the underlying physical mechanism of the impressive rate accelerations achieved by enzymes has been a central question in biology. Transition-state theory has provided the fundamental framework since the rate of a reaction is dictated by the free-energy difference between the ground and transition states (Truhlar, 2015). A wealth of research has led to the general notion that enzymatic rate acceleration is due to the enzymes' much higher affinity to the transition state (TS) relative to its substrates. This idea has been supported experimentally by the high affinities measured for transition-state analogues (TSA) relative to substrates, leading to the design of TSA as high-affine enzyme inhibitors (Lienhard, 1973; Schramm, 2007). Since the TS represents a maximum in the free-energy landscape, its structure cannot be determined directly due to its low probability and ephemeral nature, TSA-bound species have been extensively used as

structural proxies.

The classic transition-state theory and structural visualization of enzyme/TSA complexes lead to a current view of quite unique structures on the dividing surface at the maximum in the free-energy landscape. In contrast, it is now generally accepted that proteins are large ensembles of conformations, a concept rooted in pioneering work by Frauenfelder and coworkers for protein function, in analogy to the ensemble/funnel concept of protein folding (Frauenfelder & Wolynes, 1985). Consequently, enzyme-substrate (ES) complexes - experimentally accessible as minima in the free-energy landscape - are composed of a vast ensemble of molecular configurations due to their macromolecular nature. Hence, catalysis by pathing through exclusive TS's would pose a huge entropic bottleneck/energy barrier for enzyme-catalyzed reactions.

Motivated by this consideration, together with the marginal outcomes in current enzyme design relative to the catalytic power of naturally evolved enzymes, we set out to investigate the atomistic nature of transition states of the chemical step in an enzymatic cycle and its implication for rate acceleration by combining quantum-mechanics/molecular-mechanics (QM/MM) calculations and experiments. We take advantage of the groundbreaking work on TS theory by QM simulation developed in the field (Kamerlin et al., 2013; Masgrau & Truhlar, 2015; Warshel & Bora, 2016; Zinovjev & Tuñón, 2017), well summarized in several reviews (Cui, 2016; Senn & Thiel, 2009; van der Kamp & Mulholland, 2013). We chose a phosphoryl-transfer (P-transfer) reaction due to its impressive enzymatic rate acceleration, as the uncatalyzed reactions have extremely high energy barriers (Kerns et al., 2015; Lassila et al., 2011). The chemical rationale for these high barriers and reasons as to why P-transfer reactions are ubiquitous in living organisms and are involved in almost all essential biological processes is elegantly discussed in a

71 fundamental paper by Westheimer in 1987: “Why nature chose phosphates” (Westheimer,
72 1987). The central role of enzyme-catalyzed P-transfer reactions in biology (i.e., genetic
73 code, energy storage, signaling, and compartmentalization) has led to extensive
74 discussions and controversies of how enzymes catalyze these vital reactions so efficiently
75 (Allen & Dunaway-Mariano, 2016; Kamerlin et al., 2013; Kerns et al., 2015; Lassila et al.,
76 2011; Pabis et al., 2016; Westheimer, 1987). Here, we combine QM/MM calculations with
77 experimental temperature- and pH-dependent kinetic studies and X-ray crystallography of
78 adenylate kinase (Adk) to shed light on the question of transition-state structures for the
79 chemical step in its catalytic cycle. While QM/MM methods have been extensively applied
80 to study enzymatic reactions, yielding accurate and detailed descriptions of the molecular
81 events during catalysis (Acevedo & Jorgensen, 2010; Cheng et al., 2005; Dinner et al.,
82 2001; Hahn et al., 2015; Hirvonen et al., 2020; Karplus & Kuriyan, 2005; Lai & Cui, 2020a;
83 López-Canut et al., 2011; Mones et al., 2013; Palermo et al., 2015; Rosta et al., 2014;
84 Roston et al., 2018; Roston & Cui, 2016; Schwartz & Schramm, 2009; Senn & Thiel, 2009;
85 Turjanski et al., 2009), we test here the reaction free-energy profiles from simulations
86 subsequently by designed experiments. We deliver a revised notion of transition-state
87 stabilization by the enzyme through our discovery of a structurally broad transition-state
88 ensemble (TSE).

89

90 **Results**

91 Adk is an extensively studied phosphotransferase that catalyzes the reversible, roughly
92 isoenergetic conversion of two ADP molecules into ATP and AMP (Figure 1a,b), thereby
93 maintaining the cellular concentrations of these nucleotides (Dzeja & Terzic, 2009). It is an

94 essential enzyme found in every cell and organism. Extensive structural, dynamic and
95 kinetic studies led to a comprehensive picture of the overall Adk reaction mechanism and
96 its underlying energy landscape (Figure 1a) (Beckstein et al., 2009; Berry et al., 1994,
97 2006; Henzler-Wildman et al., 2007; Kerns et al., 2015; Müller et al., 1996; Müller & Schulz,
98 1992; Wolf-Watz et al., 2004). The conformational change of the AMP- and ATP-lids
99 closing and opening is crucial in the enzymatic cycle: Lid-closing positions the two
100 substrates and the active-site residues for efficient chemistry (i.e., P-transfer) and prohibits
101 the alternative, energetically favorable reaction of phosphoryl hydrolysis (Kerns et al.,
102 2015). Lid-opening, essential for product release, and not P-transfer is the rate-limiting
103 step in the catalytic cycle and Mg^{2+} accelerates both steps (Kerns et al., 2015). Ironically,
104 the piece missing to understand the enzyme's catalytic power is the mechanism of the
105 actual P-transfer step, which would take about 7000 years without the enzyme
106 (Stockbridge & Wolfenden, 2009) compared to > than 5,000 s^{-1} with the enzyme (Kerns et
107 al., 2015).

108 **QM/MM calculations of the P-transfer step in Adk**

109 In order to shed light on the mechanism by which Adk from *Aquifex aeolicus* catalyzes
110 the phosphoryl-transfer reaction by more than 12 orders of magnitude (Kerns et al., 2015),
111 we performed QM/MM simulations starting with two ADP molecules and Mg^{2+} bound in the
112 active site. The starting structures for the simulations were prepared using the X-ray struc-
113 ture of Adk in complex with Ap5A (P1,P5-Di(adenosine-5′) pentaphosphate) and coordi-
114 nated to Zn^{2+} (2RGX (Henzler-Wildman et al., 2007)). ADP-ADP coordinates were built us-
115 ing Ap5A as a template and Zn^{2+} was replaced by Mg^{2+}. For the QM/MM simulations, the
116 QM region was defined as the diphosphate moiety of both ADP molecules, the Mg^{2+} ion,
117 plus the four coordinating water molecules. The rest of the system was described at mo-

118 lecular mechanics level using the AMBER ff99sb force field (Hornak et al., 2006) and was
119 solvated with TIP3P water molecules (Figure 1 – figure supplement 1).
120 The equilibrated starting structures agree well with the X-ray structures of the enzyme
121 bound to Mg^{2+}/ADP (4CF7 (Kerns et al., 2015) Figure 1 – supplement 2). Ten simulations
122 were run in both the forward (ADP/ADP to ATP/AMP) and reverse direction (ATP/AMP to
123 ADP/ADP) with Mg^{2+} present in the active site (Figure 1 – supplement 3). Since it is
124 unknown whether the fully charged or monoprotonated nucleotide (on one β–ADP oxygen)
125 state is the more reactive configuration, we performed QM/MM simulations for both cases.
126 Free-energy profiles of the P-transfer were determined using Multiple Steered Molecular
127 Dynamics and Jarzynski's Relationship (Crespo et al., 2005; Jarzynski, 1997; Ramírez et
128 al., 2014) (Figure 1c, and Figures 1 – supplements 3-5). The results reveal a much smaller
129 free energy of activation for the fully charged nucleotide state ($\Delta_f G^{\ddagger}$ of 13 ± 0.9 kcal/mol)
130 relative to monoprotonated state ($\Delta_f G^{\ddagger}$ of 23 ± 0.9 kcal/mol) (Table 1); hence, we conclude
131 that this is the most reactive enzyme configuration.

132 When the calculations were repeated in the absence of Mg^{2+} (with the nucleotide
133 monoprotonated, since the fully-charged nucleotide state prohibited the reaction), a large
134 increase in the free energy activation barrier was observed relative to the Mg^{2+} bound
135 system (Figure 1c and Figure 1 – supplement 5, $\Delta_f G^{\ddagger}$ of 34 ± 1.6 kcal/mol), in agreement
136 with expectations from experiments (Kerns et al., 2015). We note that only a lower limit for
137 the overall acceleration by Mg^{2+} (>10^5-fold) could be estimated from published results
138 (Kerns et al., 2015), since the P-transfer was too fast to be measured experimentally in the
139 presence of Mg^{2+}.

140 **The Transition-State Ensemble (TSE) – transferring phosphoryl group delocalized**

141 The nature of the transition state of enzyme-catalyzed P-transfer reaction with respect
142 to its associative and dissociative character has been of significant interest and heated
143 debate (Kamerlin et al., 2013; Kamerlin & Wilkie, 2007; Lassila et al., 2011; Roston & Cui,
144 2016). The definition as well as theoretical and experimental approaches to distinguish
145 between them are rooted in elegant and fundamental work on *nonenzymatic* P-transfer
146 reactions (Duarte et al., 2015; Hengge, 2002; Hou et al., 2012; Hou & Cui, 2012; Kamerlin
147 et al., 2013; Kerns et al., 2015; Kirby & Nome, 2015; Stockbridge & Wolfenden, 2009). For
148 Adk, a concerted mechanism is observed with no intermediates (Figures 1c and 2).
149 Instead of using the classification of associative versus dissociative character (Lassila et
150 al., 2011), we rather apply the clear definition by Cui and coworkers of a tight versus loose
151 TS for concerted P-transfer reactions as they are unambiguously related to the bond-order
152 in the transition state (Lai & Cui, 2020a, 2020b; Roston et al., 2018; Roston & Cui, 2016).
153 For Adk, a contraction of the active site is observed while passing through the TSE, as
154 captured by the decrease in the distance between acceptor and leaving group during the
155 transition (Figures 1d and 1e). In the absence of Mg^{2+}, the acceptor and donor need to be
156 within 4 Å for the reaction to occur (Figure 1d) whereas in the presence of Mg^{2+} an
157 acceptor-donor distance of 4.5 Å is sufficient (Figure 1e). The character of the TSE can
158 best be seen from the widely used Moore-O'Ferrall-Jencks diagram (Jencks, 2002;
159 O'Ferrall, 1970) that plots the distance from the transferring phosphate to the oxygen of the
160 donor and acceptor, respectively (Figure 2). The TSE changes from tight/synchronous
161 without Mg^{2+} (meaning high bond-order for both bonds between transferring phosphate to
162 the leaving group and the attacking nucleophile) into loose with Mg^{2+} (lower bond-order for
163 these two bonds; Figures 2 and 3) (Lai & Cui, 2020a, 2020b; Roston et al., 2018; Roston &
164 Cui, 2016).

165 Importantly, from these two-dimensional (Figure 2) and the one-dimensional (Figure 1c)
166 free energy plots, we noticed a novel striking feature: a large ensemble of conformations in
167 the TS region with vast differences in the position of the transferring phosphate but equal
168 values in free energy for the enzyme with Mg^{2+} (light blue dots in Figure 2a, yellow area in
169 Figure 1c). In other words, the enzyme seems to operate with a wide TSE. In contrast,
170 without Mg^{2+} fewer conformations seem to comprise the TSE. To dive more into this
171 unexpected computational result and better visualize the TSE, we show zoom-ins of
172 representative TSE snapshots and their superposition (Figure 3 and Figure 3 –
173 supplement 1). Notably, the TSE conformations are distributed along the reaction
174 coordinate. The difference in position of the transferring phosphate along the reaction
175 coordinate within the TSE (about 1 Å with Mg^{2+}; Figures 1c, 2a, and 3b) implies that the
176 TSE contains many highly asymmetric conformations, meaning that the transferring
177 phosphate can be much closer to the leaving oxygen than the attacking oxygen and vice
178 versa (Figure 3d). This asymmetry is logically tied with nonplanar configurations of the
179 transferring phosphate (Figure 3d and Table 1).

180 Comparison of the TSE snapshots for the fully active, Mg^{2+}-bound enzyme obtained
181 from QM/MM with an X-ray structure of the same enzyme in complex with the transition-
182 state analogue (ADP- Mg^{2+}-AlF_4–AMP) (Kerns et al., 2015) serves as an initial
183 experimental validation of our simulations (Figures 3e,f and Figure 3 – supplement 2). At
184 the same time, this comparison highlights the power of the QM/MM simulations to
185 investigate the catalytic mechanism, as the TSA-bound X-ray structure seems to imply
186 quite a unique TS conformation, in sharp contrast to the broad TSE discovered in our
187 simulations.

188 A detailed analysis of the pathways with and without Mg^{2+} reveals well-known features

189 from other P-transfer enzymes, such as coordinated changes of the Mulliken charge
190 populations coupled with proton transfers (Figure 1 – supplements 6-8). Mg^{2+} achieves its
191 catalytic effect on the chemical step playing several roles. It enables the donor and
192 acceptor phosphates to come close enough to react, thus achieving a reactive
193 conformation. In the absence of Mg^{2+}, a proton must bridge the terminal phosphates to
194 prevent the strong electrostatic repulsion between the two nucleotides. In addition, Mg^{2+}
195 stabilizes the charge of the transferring phosphate and thereby lowering the enthalpic
196 barrier. Most interestingly, the presence of a cation seems to result in a wide TSE.
197 Structures of the transition-state ensemble show that Mg^{2+} is optimally coordinated to the
198 transferring phosphates and water molecules.

199 Besides the multifaceted role of Mg^{2+}, our simulations provide insights into the function
200 of the fully-conserved arginine residues in the active site for lowering the activation barrier
201 for this chemical reaction (Figure 3 – supplements 3-5). R85 appears to arrange the β-
202 phosphates of the ADPs in the proper position for the reaction to be started. R150 and
203 R161 are involved in anchoring ATP and AMP residues in the backward reaction. These
204 last two residues and R85 interact with the Pα of AMP, stabilizing its negative charge. R36
205 is near to the α-phosphate of AD(M)P along the entire catalytic reaction, stabilizing both
206 the transition state and products. Overall, interactions between these arginine side chains
207 and several backbone amides and the Mg^{2+} with the phosphates of the substrate make up
208 a well-organized, asymmetric active site enabling efficient reversible P-transfer with a wide
209 TSE (Figure 3g).

210 Stimulated by experts in the field that keep pushing the methodology, we tested the
211 accuracy and robustness of our results from our original QM/MM level of theory by
212 employing higher level pure DFT (PBE) free energy calculations similar to the approaches

213 used by Ganguly et al. (Ganguly et al., 2020) (Figure 1 – supplement 9). The results are in
214 excellent agreement with the free energy profiles obtained before (Figures 1a,e and
215 Figures 2a,c) thus further supporting the computational results.

216 **Experimental characterization of the activation parameters of the P-transfer step**

217 We felt the need to experimentally test our major new finding from the QM/MM
218 simulations: a delocalized TSE. This feature would result in a lowering of the entropic
219 barrier for the chemical step, thereby contributing to the enzyme-catalyzed rate
220 enhancement. To avoid the issues of accuracy of QM/MM simulations that are well
221 documented (Acevedo & Jorgensen, 2010; Elstner, 2007; Gaus et al., 2014; Roston et al.,
222 2018), our system has the advantage of comparing the exact same reaction coordinate
223 with the only difference being the presence/absence of a single atom, Mg^{2+}, thereby
224 studying differences rather than absolute values. Since the reaction with Mg^{2+} (fully active
225 enzyme) revealed a more pronounced delocalization than the reaction in its absence, the
226 divalent cation is predicted to lower the activation entropy. To test this prediction, we
227 experimentally determined the enthalpic and entropic contributions to the chemical
228 reaction barrier in Adk by measuring its temperature dependence in the presence and
229 absence of Ca^{2+}. The experimental trick of replacing Mg^{2+} with Ca^{2+} was used since the
230 chemical step with Mg^{2+} is too fast to be experimentally measured, and previous studies
231 showed that Ca^{2+} is an appropriate mimic to selectively probe the chemical step (Kerns et
232 al., 2015).

233 The resulting Eyring plots for the two experiments (Figure 4a) deliver the enthalpic ($\Delta H^{\#}$
234 of 64.1 ± 2.2 and 70.0 ± 4.1 kJ/mol) and entropic ($\Delta S^{\#}$ = -23.8 ± 6.8 and -80.0 ± 12.8
235 J/mol/K) contributions to the chemical reaction barrier in the presence and absence of Ca^{2+},

236 respectively. The presence of Ca^{2+} reduces both barriers considerably. The decrease in
237 the enthalpic barrier by Ca^{2+}, which is even more pronounced with the optimal Mg^{2+} ion, is
238 not new and has been well-established in the literature for P-transfer reactions, including
239 the Adk chemical reaction (Kerns et al., 2015; Pérez-Gallegos et al., 2017; Rosta et al.,
240 2014; L. Yang et al., 2012). The striking new result, central to this work, is the large
241 decrease in the entropic barrier in the presence of a divalent cation, thereby strongly
242 supporting our key finding of a broader TSE from the QM/MM simulations.

243 We were able to further test our QM/MM simulations with a second designed set of
244 experiments by measuring the pH dependence of the P-transfer step. The reaction rate
245 increases with higher pH in the presence of Ca^{2+}, whereas without a metal the opposite
246 trend is observed (Figure 4b). These experimental results match the simulation results: the
247 fully-charged nucleotides state was the most reactive in the presence of the metal,
248 whereas the monoprotonated state had a much higher free-energy barrier. In contrast,
249 without metal only the monoprotonated nucleotides were reactive. Notably, at low pH (pH
250 5), the P-transfer step becomes rate limiting even with Mg^{2+}, allowing for an estimate of
251 the rate enhancement of Mg^{2+} versus Ca^{2+} of 24-fold.

252 Finally, we measured the forward and backward reaction rate constants of several
253 arginine mutants that were identified as important for the P-transfer from the QM/MM
254 simulations: R36K, R85K, R124K, R150K, and R161K (Table 2). The large decrease in the
255 catalytic rate for each single Arg to Lys mutation further highlights the notion of a highly-
256 choreographed active site for a well-coordinated P-transfer (Figure 3g), in which arginine
257 residues that are not even directly coordinated to the transferring phosphate play an
258 equally important role.

Discussion

Adk is an impressively efficient enzyme, being able to accelerate the P-transfer reaction over a billion times. Previous work showed the complexity of the Adk free-energy landscape for this two-substrate, two-product reaction (Figure 1a), providing direct experimental evidence for the widely accepted concept of a multidimension free energy landscape with multiple intermediates and transitions states for the full enzymatic cycle, already well described and demonstrated by Benkovic and Hammes-Schiffer (Benkovic et al., 2008). Full lid-closure results in an excellent preorientation of the donor and acceptor groups of the two bound nucleotides and the aiding active site residues in the enzyme/substrate complex, in agreement with the general view of necessary preorganization in enzyme catalysis. Lid-opening had been identified as the rate-limiting step in the enzymatic cycle (Kerns et al., 2015), and the corresponding TSE for this conformational change (Stiller et al., 2019) and the next intermediate, the EP complex before product dissociation (Stiller et al., 2022), recently been described.

However, for a comprehensive understanding of the complete free-energy landscape of Adk catalysis, the key step, catalyzing the actual chemical step of P-transfer, had been missing. While ES and EP complexes such as Adk bound to ADP/Mg^{2+} can be structurally characterized by traditional experimental methods as they represent a minimum in the free-energy landscape, the reaction path from substrate to product involving breaking and forming covalent bonds (chemical step) and traversing the crucial transition state can only be “visualized” by Quantum mechanics based molecular simulations. The power of such simulations to examine the chemical steps in enzymes, including P-transfer reactions, has been extensively documented (Jin et al., 2017; Lai & Cui, 2020b; Mokrushina et al., 2020; Pérez-Gallegos et al., 2015, 2017; Roston & Cui, 2016; Valiev et al., 2007). The focus in

283 the literature has been on the comparison of the enzyme-catalyzed and uncatalyzed reac-
284 tion with respect to the bond character at the transitions state (i.e., associate versus disso-
285 ciative or tight versus loose) (Admiraal & Herschlag, 1995; Hengge, 2002; Kamerlin et al.,
286 2013; Lassila et al., 2011). Here, we uncover a central new result that provokes a modified
287 transition-state theory. Enzymes, due to their macromolecular nature, provide a fundamen-
288 tally different, advantageous way to catalyze these chemical reactions compared to the
289 uncatalyzed reaction by employing a broad TSE. Many different molecular configurations
290 can be accommodated in the transition-state region with comparable energies via collec-
291 tive motions, spanning a 1 Å range along the reaction coordinate for the transferring phos-
292 phate that travels a total distance of only 2 Å during the P-transfer. This features resem-
293 blance the now well-established conformational sampling of proteins in ground states such
294 as ES complexes. Our findings explain why enzymes do not face an entropic bottleneck
295 for catalysis. Furthermore, as enzyme active sites are asymmetric in contrast to the sym-
296 metric nature of the solvent for uncatalyzed reactions, we find that the TSE comprises also
297 highly asymmetric conformations. Our findings help resolve the controversy about the na-
298 ture of the transition state in enzyme-catalysed P-transfer reactions between theory and
299 experiments (Lassila et al., 2011). The complex nature of the active site of enzymes, in
300 contrast to simple solvent, results in different mechanisms in the enzyme catalyzed reac-
301 tion. We further note that a previous QM/MM minimum energy path calculations for Adk
302 using a semiempirical method had proposed a different mechanism with a stable meta-
303 phosphate intermediate with an even lower energy for this metaphosphate intermediate
304 than the ES- and EP-complexes (Shibanuma et al., 2020). In complex systems, such as
305 enzymes, it is possible to observe artificial local minima when using minimum energy path
306 searching strategies due to inadequate sampling (Mendieta-Moreno et al., 2015; Quesne
307 et al., 2016). From our NMR and x-ray experimental data we know that such stable meta-

phosphate does not exist in Adk-catalyzed reactions, highlighting the importance of experimental verification of simulations as performed here, and the use of extensive sampling with proper thermodynamic treatment.

A wide TSE agrees with the definition of the TS being a surface on the potential energy surface instead of a saddle as elegantly discussed in a theoretical paper by Nussinov and colleagues (Ma et al., 2000). Our results deliver concrete evidence for this fundamental concept from the free-energy profiles of the QM/MM calculations on Adk that were further buttressed by the consequently designed experiments. Although we have only quantitatively demonstrated this TSE concept here for Adk catalyzed P-transfer, we hypothesize such mechanism to be more general for enzyme catalysis as it is rooted in the macroscopic nature of proteins. A conformationally spread-out TSE is likely one reason why enzymes are much bigger than a few active-site residues: On one hand residues remote from the site of the chemical action allow for conformational flexibility without the protein unfolding, on the other hand they allow for increasing the probability of highly-choreographed motions along the reaction coordinate (Hammes-Schiffer & Benkovic, 2006; Klinman & Kohen, 2013; Saen-Oon et al., 2008; Schramm & Schwartz, 2018) while reducing excursions into unproductive conformations (Otten et al., 2020). The latter is directly demonstrated here in the TSE as the configurations seen in the simulations are along the P-transfer reaction coordinate. We note that we focus here on equilibrium effects and an atomistic description of the TSE, this is not related to the fundamental work on dynamical effects manifested in transmission coefficients due to barrier recrossing (Antoniou & Schwartz, 2016; Zinovjev & Tuñón, 2017). The latter has been quantitatively demonstrated to play a minor role.

A question often being asked is why would nature evolve a conformational step to be rate limiting, as the lid-opening step for Adk? We propose that this is the “price” the

333 enzyme pays for stabilizing the ES complex to enable efficient rate acceleration of the
334 chemical step and for suppressing detrimental alternate reactions such as phosphate
335 hydrolysis. Release of product requires disassembly of such closed, low-energy structure.
336 These principles have now been directly revealed on an atomic scale for Adk: extensive
337 electrostatic interactions of 5 Arg and one Lys with the phosphoryl groups to efficiently
338 accelerate the P-transfer step, which then need to be broken for lid opening to allow
339 product release. However, as long as the rate of this conformational transition (k_{open}) and
340 hence k_{cat} is not limiting for organismal fitness, there is no evolutionary pressure to further
341 enhance it.

342 The importance of TSE including multiple transition pathways for protein folding
343 (Frauenfelder et al., 2006; Royer, 2008), and more recently for protein conformational
344 transitions within the folded state (Pontiggia et al., 2015; Stiller et al., 2019; Tsai &
345 Nussinov, 2014) has been well documented. TSE in enzyme catalysis of chemical steps
346 where covalent bonds are broken and formed as demonstrated now here further promotes
347 a unifying concept of protein folding and function, as the same principal concept of TSE is
348 seen for these different types of conformational changes. Each protein is uniquely
349 described by the corresponding free energy landscape that includes folded and unfolded
350 conformational substates and is defined by the amino acid sequence and the surrounding
351 solvent. Consequently, protein folding and function is embedded in a unifying energy
352 landscape which is simply altered by ligands and solvent.

353

354 **Materials and Methods**

355 **Computational Set up of the system.** The crystal structure of adenylate kinase from *Aq-*
356 *uifex aeolicus* in complex with Ap5A coordinated to Zn^{2+} (PDB ID 2RGX (Henzler-Wildman
357 et al., 2007)) was used as model. The Zn^{2+} ion was replaced by Mg^{2+} and the ADPs struc-
358 tures were built by modifying the structure of Ap5A, keeping the crystallographic coordina-
359 tion of the cation (2 oxygens from ADPs and 4 waters). For the simulation in low pH and
360 without magnesium ion, the nucleophilic oxygen of AD(T)P was protonated. Standard pro-
361 tonation states were assigned to all titratable residues (aspartate and glutamate residues
362 are negatively charged, lysines and arginines residues are positively charged). Histidine
363 protonation was assigned favoring formation of hydrogen bonds in the crystal structure.
364 Each protein was immersed in a truncated octahedral box of TIP3P water (Jorgensen et
365 al., 1983). The parameters used for the protein were those corresponding to AMBER force
366 field ff99sb (Hornak et al., 2006). For the non-protein residues, as ADP and Mg^{2+}, the pa-
367 rameters were taken from refs. Meagher et al. (Meagher et al., 2003) and Allnér et al.
368 (Allnér et al., 2012).

369 **Simulation Parameters**. (a) Classical force field and Scheme: All simulations were
370 performed with periodic boundary conditions; the SHAKE algorithm was used to retain the
371 hydrogen atoms at equilibrium bond lengths, allowing the use of a 2 fs time step. Pressure
372 and temperature were kept constant with the Berendsen barostat and thermostat,
373 respectively (Berendsen et al., 1984). All the simulations were equilibrated following the
374 same protocol: 1) 2000 steps of optimization using a conjugate gradient algorithm; 2) 100
375 ps MD simulation at NVT condition where the system's temperature was slowly raised to
376 300 K; 3) 100 ps MD simulation at NPT conditions to equilibrate the system's density. The
377 protein *α*-carbon atoms were restrained by a 10 kcal mol^{-1} harmonic potential for the
378 thermalization and by a 1 kcal mol^{-1} harmonic potential for the density equilibration.
379 Afterwards, a production simulation was performed for 7.5 ns at NPT conditions. (b)

380 QM/MM parameters: QM/MM simulations were performed starting from selected snaphots
381 from the classical production simulation. To equilibrate the system with the QM/MM
382 hamiltonian, we performed first a conjugate gradient QM/MM optimization, followed by a
383 50 ps QM/MM MD equilibration process, subsequently each production simulation was
384 performed. QM/MM calculations were performed using the additive scheme implemented
385 in the sander module of the AMBER program suite (Case et al., 2005). The quantum (QM)
386 region was treated with the self-consistent charge-density functional tight-binding (SCC-
387 DFTB) approach (Elstner, 2007), usually considered a semi-empirical QM method, as
388 implemented in Sander (Seabra et al., 2007; Walker et al., 2008). The SCC-DFTB
389 parameter set involving carbon, hydrogen, oxygen, nitrogen, phosphate, and magnesium
390 was employed throughout this study (Cai et al., 2007; Y. Yang et al., 2008). All the other
391 atoms were described with AMBER ff99SB force field (Hornak et al., 2006). The interface
392 between the QM and MM portions of the system was treated with the scaled position-link
393 atom method. The QM region of the complete system consisted of the diphosphate moiety
394 of both ADP molecules, one Mg^{2+} ion, and the four water molecules that coordinate the
395 metal ion in the crystal structure (Figure 1 – supplement 1).

396 **Free energy determination strategy.** The free-energy profiles were constructed by
397 performing constant velocity multiple steered molecular dynamics (MSMD) simulations (i.e.,
398 stiff string approximation), and using Jarzynski's equality (Jarzynski, 1997), which relates
399 equilibrium free-energy values with the irreversible work performed over the system along
400 a user defined reaction coordinate that drives the system from reactants to products. In the
401 present study, the reaction coordinate (ξ) was chosen as:

402 $$\xi = d(O_{leaving}\text{-}P) - d(O_{attacking}\text{-}P) \quad (1)$$

403 Calculations were performed using a force constant of 300 kcal mol^{-1} $Å^{-1}$ and pulling ve-
404 locities of 0.05 Å ps^{-1}. To reconstruct the free-energy profile of the phosphate transfer re-
405 action, two sets of 10 SMD runs were performed starting from equilibrated QM/MM MD
406 structures corresponding to either the system in 1) the Adk/ADP-ADP state (for forward
407 reaction), and 2) the Adk/ATP-AMP state (for backward reaction). Each set of work profiles
408 was used to obtain the corresponding forward and back free-energy profiles with Jarzyn-
409 ski's equality (Jarzynski, 1997), and finally the two profiles were combined to obtain the
410 complete curve. This strategy was successfully used to obtain enzymatic reaction free-
411 energy profiles in previous works (Crespo et al., 2005; Defelipe et al., 2015). The ADP in
412 the ATP-lid will be called as AD(T)P and the other, in the AMP-lid, as AD(M)P. The reac-
413 tion involves the two P-O bonds, one forming and the another breaking, the two bonds
414 sharing the same phosphorus atom from the transferring phosphate (Figure 1b). In the
415 former, an oxygen atom of the AD(T)P reacts and we will name it as $O_{attacking}$. The breaking
416 bond is described by the oxygen atom for the AD(M)P and it will be called $O_{leaving}$.
417
418 **Higher level DFT(PBE) free energy calculations.** The free-energy profile of the ADK
419 with Mg^{2+} was also computed using a higher level of theory. Here, the QM system was
420 described with PBE functional (Perdew et al., 1996) using a DZVP basis set as
421 implemented in the GPU based code LIO that works with amber (Nitsche et al., 2014). To
422 take advantage of previous DFTB sampling, five lowest work vs RC profiles of the forward
423 and back reaction were selected, and segmented in 10 windows or stages. For each
424 window, the free energy profile at the DFT(PBE) level was computed using SMD with a
425 steering velocity of 0.05 Å/ps. Windows were combined to obtain both forward and back
426 FEP and the final profile was obtained by joining them. Details of the staged strategy can
427 be found in references Ozer et al. (Ozer et al., 2010, 2012) and Ganguly et al. (Ganguly et

428 al., 2020).

429 **Steady-state kinetics measurements.** Steady-state kinetics measurements for *Aquifex*
430 *aeolicus* Adk (Adk) were performed at different pH values in the absence of divalent met-
431 als (using 50 mM of EDTA) and the presence of Mg^{2+} or Ca^{2+}. In all cases the reaction was
432 started by the addition of 8 mM ADP and saturating metal concentrations were used if ap-
433 plicable (32 mM at pH 5 and 8 mM at pH 7 and 9, respectively). The enzyme concentration
434 varied between 30 nM and 200 μM depending on the rate of interconversion; measure-
435 ments were collected at 25 ºC. The amount of product was quantified with high-pressure
436 liquid chromatography (HPLC). Protein precipitated by quench (30% TCA + 6 M HCl mix-
437 ture) was separated with Spin-X centrifugal tube filters (Costar), filtered supernatant was
438 diluted to avoid HPLC detector saturation, and the pH was brought to 6.0 to achieve opti-
439 mal separation. The samples were analyzed on an HPLC system (Agilent Infinity 1260)
440 with a high-precision autosampler (injection error <0.1 μL) and analytical HPLC column
441 ACE (i.d. 2.4 mm, length 250 mm, C18-AR, 5 Å pore size) and separated with isocratic
442 elution with potassium phosphate mobile phase (100 mM, pH 6.1). The observed rate con-
443 stants were determined from 8 – 15 data points for each temperature and/or pH value us-
444 ing initial rate analysis. The values and uncertainties (s.d.) shown in Figure 4 and Table 2
445 were determined from least-squares linear regression. Similarly, values and uncertainties
446 (s.d.) of $\Delta H^{\ddagger}$ and $\Delta S^{\ddagger}$ were extracted from linear regression of the data points presented in
447 Figure 4a.

448 **Temperature Dependence of catalysis and Mutant activity.** Experiments were essen-
449 tially performed as described previously[6] and above. In short, the steady-state kinetics
450 measurements were collected at temperatures between 20 and 60 °C for the temperature-
451 dependency and at 25 °C for the mutants. For the temperature dependence, the samples

452 contained 4 mM ADP and equimolar (with nucleotide) concentrations of calcium or 50 mM
453 EDTA. The enzyme concentration was varied between 50 nM – 1 μM (with Ca^{2+}) or 100 –
454 200 μM (with EDTA); buffer was 100 mM HEPES, pH 7.0, and 80 mM KCl. The amount of
455 product produced over time (10-16 minutes) was quantified with HPLC and observed rates
456 were extracted as described above. A similar approach was used for the Arg-to-Lys Aadk
457 mutants, where the reaction was measured in both directions starting with either 4 mM
458 ADP or ATP/AMP and equimolar (with nucleotide) concentrations of Mg^{2+}.

459 **Acknowledgment**

460 This work was supported by the Howard Hughes Medical Institute (HHMI) to D.K. We
461 thank to "High-Performance Computing Center" (CeCAR, https://cecar.fcen.uba.ar/) of the
462 *Facultad de Ciencias Exactas y Naturales* at the University of Buenos Aires for the
463 computational resources.

464 **Competing interests:** D.K. is co-founder of Relay Therapeutics and MOMA Therapeutics.
465 The remaining authors declare no competing interests.

466

References

Acevedo, O., & Jorgensen, W. L. (2010). Advances in Quantum and Molecular Mechanical (QM/MM) Simulations for Organic and Enzymatic Reactions. *Accounts of Chemical Research*, *43*(1), 142–151. https://doi.org/10.1021/ar900171c

Admiraal, S. J., & Herschlag, D. (1995). Mapping the transition state for ATP hydrolysis: Implications for enzymatic catalysis. *Chemistry & Biology*, *2*(11), 729–739. https://doi.org/10.1016/1074-5521(95)90101-9

Allen, K. N., & Dunaway-Mariano, D. (2016). Catalytic scaffolds for phosphoryl group transfer. *Current Opinion in Structural Biology*, *41*, 172–179. https://doi.org/10.1016/j.sbi.2016.07.017

Allnér, O., Nilsson, L., & Villa, A. (2012). Magnesium Ion–Water Coordination and Exchange in Biomolecular Simulations. *Journal of Chemical Theory and Computation*, *8*(4), 1493–1502. https://doi.org/10.1021/ct3000734

Antoniou, D., & Schwartz, S. D. (2016). Phase Space Bottlenecks in Enzymatic Reactions. *The Journal of Physical Chemistry B*, *120*(3), 433–439. https://doi.org/10.1021/acs.jpcb.5b11157

Beckstein, O., Denning, E. J., Perilla, J. R., & Woolf, T. B. (2009). Zipping and Unzipping of Adenylate Kinase: Atomistic Insights into the Ensemble of Open ??? Closed Transitions. *Journal of Molecular Biology*, *394*(1), 160–176. https://doi.org/10.1016/j.jmb.2009.09.009

Benkovic, S. J., Hammes, G. G., & Hammes-Schiffer, S. (2008). Free-Energy Landscape of Enzyme Catalysis. *Biochemistry*, *47*(11), 3317–3321. https://doi.org/10.1021/bi800049z

Berendsen, H. J. C., Postma, J. P. M., Van Gunsteren, W. F., Dinola, A., & Haak, J. R. (1984). Molecular dynamics with coupling to an external bath. *The Journal of Chemical Physics*, *81*(8), 3684–3690. https://doi.org/10.1063/1.448118

Berry, M. B., Bae, E., Bilderback, T. R., Glaser, M., & Phillips, G. N. (2006). Crystal

structure of ADP/AMP complex of Escherichia coli adenylate kinase. *Proteins*, *62*(2), 555–556. https://doi.org/10.1002/prot.20699

Berry, M. B., Meador, B., Bilderback, T., Liang, P., Glaser, M., & Phillips, G. N. (1994). The closed conformation of a highly flexible protein: The structure of E. coli adenylate kinase with bound AMP and AMPPNP. *Proteins: Structure, Function and Genetics*, *19*(3), 183–198. https://doi.org/10.1002/prot.340190304

Cai, Z.-L., Lopez, P., Reimers, J. R., Cui, Q., & Elstner, M. (2007). Application of the Computationally Efficient Self-Consistent-Charge Density-Functional Tight-Binding Method to Magnesium-Containing Molecules †. *The Journal of Physical Chemistry A*, *111*(26), 5743–5750. https://doi.org/10.1021/jp071701m

Case, D. A., Cheatham, T. E., Darden, T., Gohlke, H., Luo, R., Merz, K. M., Onufriev, A., Simmerling, C., Wang, B., & Woods, R. J. (2005). The Amber biomolecular simulation programs. *Journal of Computational Chemistry*, *26*(16), 1668–1688. https://doi.org/10.1002/JCC.20290

Cheng, Y., Zhang, Y., & McCammon, J. A. (2005). How does the cAMP-dependent protein kinase catalyze the phosphorylation reaction: An ab Initio QM/MM study. *Journal of the American Chemical Society*, *127*(5), 1553–1562. https://doi.org/10.1021/ja0464084

Crespo, A., Mart??, M. A., Estrin, D. A., & Roitberg, A. E. (2005). Multiple-steering QM-MM calculation of the free energy profile in chorismate mutase. *Journal of the American Chemical Society*, *127*(19), 6940–6941. https://doi.org/10.1021/ja0452830

Cui, Q. (2016). Perspective: Quantum mechanical methods in biochemistry and biophysics. *The Journal of Chemical Physics*, *145*(14), 140901. https://doi.org/10.1063/1.4964410

Defelipe, L. A., Lanzarotti, E., Gauto, D., Marti, M. A., & Turjanski, A. G. (2015). Protein Topology Determines Cysteine Oxidation Fate: The Case of Sulfenyl Amide Formation among Protein Families. *PLOS Computational Biology*, *11*(3), e1004051. https://doi.org/10.1371/journal.pcbi.1004051

Dinner, A. R., Blackburn, G. M., & Karplus, M. (2001). Uracil-DNA glycosylase acts by substrate autocatalysis. *Nature*, *413*(6857), 752–755. https://doi.org/10.1038/35099587

Duarte, F., Åqvist, J., Williams, N. H., & Kamerlin, S. C. L. (2015). Resolving Apparent Conflicts between Theoretical and Experimental Models of Phosphate Monoester Hydrolysis. *Journal of the American Chemical Society*, *137*(3), 1081–1093. https://doi.org/10.1021/ja5082712

Dzeja, P., & Terzic, A. (2009). Adenylate kinase and AMP signaling networks: Metabolic monitoring, signal communication and body energy sensing. *International Journal of Molecular Sciences*, *10*(4), 1729–1772. https://doi.org/10.3390/ijms10041729

Elstner, M. (2007). SCC-DFTB: What is the proper degree of self-consistency. *Journal of Physical Chemistry A*, *111*(26), 5614–5621. https://doi.org/10.1021/jp071338j

Frauenfelder, H., Fenimore, P. W., Chen, G., & McMahon, B. H. (2006). Protein folding is slaved to solvent motions. *Proceedings of the National Academy of Sciences of the United States of America*, *103*(42), 15469–15472. https://doi.org/10.1073/pnas.0607168103

Frauenfelder, H., & Wolynes, P. G. (1985). Rate theories and puzzles of hemeprotein kinetics. *Science*, *229*(4711), 337–345. https://doi.org/10.1126/science.4012322

Ganguly, A., Weissman, B. P., Giese, T. J., Li, N.-S., Hoshika, S., Rao, S., Benner, S. A., Piccirilli, J. A., & York, D. M. (2020). Confluence of theory and experiment reveals the catalytic mechanism of the Varkud satellite ribozyme. *Nature Chemistry*, *12*(2), 193–201. https://doi.org/10.1038/s41557-019-0391-x

Gaus, M., Cui, Q., & Elstner, M. (2014). Density functional tight binding: Application to organic and biological molecules. *Wiley Interdisciplinary Reviews: Computational Molecular Science*, *4*(1), 49–61. https://doi.org/10.1002/wcms.1156

Hahn, D. K., Tusell, J. R., Sprang, S. R., & Chu, X. (2015). Catalytic Mechanism of Mammalian Adenylyl Cyclase: A Computational Investigation. *Biochemistry*, *54*(40), 6252–6262. https://doi.org/10.1021/acs.biochem.5b00655

Hammes-Schiffer, S., & Benkovic, S. J. (2006). Relating Protein Motion to Catalysis. *Annual Review of Biochemistry*, *75*(1), 519–541. https://doi.org/10.1146/annurev.biochem.75.103004.142800

Hengge, A. C. (2002). Isotope Effects in the Study of Phosphoryl and Sulfuryl Transfer Reactions. *Accounts of Chemical Research*, *35*(2), 105–112. https://doi.org/10.1021/ar000143q

Henzler-Wildman, K. a, Thai, V., Lei, M., Ott, M., Wolf-Watz, M., Fenn, T., Pozharski, E., Wilson, M. a, Petsko, G. a, Karplus, M., Hübner, C. G., & Kern, D. (2007). Intrinsic motions along an enzymatic reaction trajectory. *Nature*, *450*(7171), 838–844. https://doi.org/10.1038/nature06410

Hirvonen, V. H. A., Mulholland, A. J., Spencer, J., & van der Kamp, M. W. (2020). Small Changes in Hydration Determine Cephalosporinase Activity of OXA-48 β-Lactamases. *ACS Catalysis*, *10*(11), 6188–6196. https://doi.org/10.1021/acscatal.0c00596

Hornak, V., Abel, R., Okur, A., Strockbine, B., Roitberg, A., & Simmerling, C. (2006). Comparison of multiple Amber force fields and development of improved protein backbone parameters. *Proteins: Structure, Function, and Bioinformatics*, *65*(3), 712–725. https://doi.org/10.1002/PROT.21123

Hou, G., & Cui, Q. (2012). QM/MM analysis suggests that alkaline phosphatase (AP) and nucleotide pyrophosphatase/phosphodiesterase slightly tighten the transition state for phosphate diester hydrolysis relative to solution: Implication for catalytic promiscuity in the AP superfamil. *Journal of the American Chemical Society*, *134*(1), 229–246. https://doi.org/10.1021/ja205226d

Hou, G., Zhu, X., Elstner, M., & Cui, Q. (2012). A modified QM/MM hamiltonian with the self-consistent-charge density-functional-tight-binding theory for highly charged QM regions. *Journal of Chemical Theory and Computation*, *8*(11), 4293–4304. https://doi.org/10.1021/ct300649f

Jarzynski, C. (1997). Nonequilibrium Equality for Free Energy Differences. *Physical*

Review Letters, *78*(14), 2690–2693. https://doi.org/10.1103/PhysRevLett.78.2690

Jencks, W. P. (2002). General acid-base catalysis of complex reactions in water. *Chemical Reviews*, *72*(6), 705–718. https://doi.org/10.1021/CR60280A004

Jin, Y., Richards, N. G., Waltho, J. P., & Blackburn, G. M. (2017). Metal Fluorides as Analogues for Studies on Phosphoryl Transfer Enzymes. *Angewandte Chemie International Edition*, *56*(15), 4110–4128. https://doi.org/10.1002/anie.201606474

Jorgensen, W. L., Chandrasekhar, J., Madura, J. D., Impey, R. W., & Klein, M. L. (1983). Comparison of simple potential functions for simulating liquid water. *The Journal of Chemical Physics*, *79*(2), 926–935. https://doi.org/10.1063/1.445869

Kamerlin, S. C. L., Sharma, P. K., Prasad, R. B., & Warshel, A. (2013). Why nature really chose phosphate. *Quarterly Reviews of Biophysics*, *46*(1), 1–132. https://doi.org/10.1017/S0033583512000157

Kamerlin, S. C. L., & Wilkie, J. (2007). The role of metal ions in phosphate ester hydrolysis. *Organic and Biomolecular Chemistry*, *5*(13), 2098–2108. https://doi.org/10.1039/b701274h

Karplus, M., & Kuriyan, J. (2005). Molecular dynamics and protein function. *Proceedings Of The National Academy Of Sciences Of The United States Of America*, *102*(19), 6679–6685. https://doi.org/10.1073/pnas.0408930102

Kerns, S. J., Agafonov, R. V., Cho, Y.-J. J., Pontiggia, F., Otten, R., Pachov, D. V., Kutter, S., Phung, L. A., Murphy, P. N., Thai, V., Alber, T., Hagan, M. F., & Kern, D. (2015). The energy landscape of adenylate kinase during catalysis. *Nature Structural & Molecular Biology*, *22*(2), 124–131. https://doi.org/10.1038/nsmb.2941

Kirby, A. J., & Nome, F. (2015). Fundamentals of Phosphate Transfer. *Accounts of Chemical Research*, *48*(7), 1806–1814. https://doi.org/10.1021/ACS.ACCOUNTS.5B00072

Klinman, J. P., & Kohen, A. (2013). Hydrogen Tunneling Links Protein Dynamics to Enzyme Catalysis. *Annual Review of Biochemistry*, *82*(1), 471–496. https://doi.org/10.1146/annurev-biochem-051710-133623

Lai, R., & Cui, Q. (2020a). Differences in the Nature of the Phosphoryl Transfer Transition State in Protein Phosphatase 1 and Alkaline Phosphatase: Insights from QM Cluster Models. *The Journal of Physical Chemistry B*, *124*(42), 9371–9384. https://doi.org/10.1021/acs.jpcb.0c07863

Lai, R., & Cui, Q. (2020b). What Does the Brønsted Slope Measure in the Phosphoryl Transfer Transition State? *ACS Catalysis*, *10*(23), 13932–13945. https://doi.org/10.1021/acscatal.0c03764

Lassila, J. K., Zalatan, J. G., & Herschlag, D. (2011). Biological Phosphoryl-Transfer Reactions: Understanding Mechanism and Catalysis. *Annual Review of Biochemistry*, *80*(1), 669–702. https://doi.org/10.1146/annurev-biochem-060409-092741

Lienhard, G. E. (1973). Enzymatic Catalysis and Transition-State Theory. *Science*, *180*(4082), 149–154. https://doi.org/10.1126/science.180.4082.149

López-Canut, V., Roca, M., Bertrán, J., Moliner, V., & Tuñón, I. (2011). Promiscuity in alkaline phosphatase superfamily. Unraveling evolution through molecular simulations. *Journal of the American Chemical Society*, *133*(31), 12050–12062. https://doi.org/10.1021/ja2017575

Ma, B., Kumar, S., Tsai, C. J., Hu, Z., & Nussinov, R. (2000). Transition-state ensemble in enzyme catalysis: Possibility, reality, or necessity? *Journal of Theoretical Biology*, *203*(4), 383–397. https://doi.org/10.1006/jtbi.2000.1097

Masgrau, L., & Truhlar, D. G. (2015). The Importance of Ensemble Averaging in Enzyme Kinetics. *Accounts of Chemical Research*, *48*(2), 431–438. https://doi.org/10.1021/ar500319e

Meagher, K. L., Redman, L. T., & Carlson, H. A. (2003). Development of Polyphosphate Parameters for Use with the AMBER Force Field. *Journal of Computational Chemistry*, *24*, 1016–1025.

Mendieta-Moreno, J. I., Marcos-Alcalde, I., Trabada, D. G., Gómez-Puertas, P., Ortega, J., & Mendieta, J. (2015). A Practical Quantum Mechanics Molecular Mechanics

Method for the Dynamical Study of Reactions in Biomolecules. In *Advances in Protein Chemistry and Structural Biology* (Vol. 100, pp. 67–88). Elsevier. https://doi.org/10.1016/bs.apcsb.2015.06.003

Mokrushina, Y. A., Golovin, A. V., Smirnov, I. V., Chatziefthimiou, S. D., Stepanova, A. V., Bobik, T. V., Zalevsky, A. O., Zlobin, A. S., Konovalov, K. A., Terekhov, S. S., Stepanov, A. V., Pipiya, S. O., Shamborant, O. G., Round, E., Belogurov, A. A., Bourenkov, G., Makarov, A. A., Wilmanns, M., Xie, J., … Lerner, R. A. (2020). Multiscale computation delivers organophosphorus reactivity and stereoselectivity to immunoglobulin scavengers. *Proceedings of the National Academy of Sciences*, *117*(37), 22841–22848. https://doi.org/10.1073/pnas.2010317117

Mones, L., Tang, W.-J., & Florián, J. (2013). Empirical valence bond simulations of the chemical mechanism of ATP to cAMP conversion by anthrax edema factor. *Biochemistry*, *52*(15), 2672–2682. https://doi.org/10.1021/bi400088y

Müller, C. W., Schlauderer, G. J., Reinstein, J., & Schulz, G. E. (1996). Adenylate kinase motions during catalysis: An energetic counterweight balancing substrate binding. *Structure (London, England : 1993)*, *4*(2), 147–156. https://doi.org/10.1016/S0969-2126(96)00018-4

Müller, C. W., & Schulz, G. E. (1992). Structure of the complex between adenylate kinase from Escherichia coli and the inhibitor Ap5A refined at 1.9 Å resolution. A model for a catalytic transition state. *Journal of Molecular Biology*, *224*(1), 159–177. https://doi.org/10.1016/0022-2836(92)90582-5

Nitsche, M. A., Ferreria, M., Mocskos, E. E., & González Lebrero, M. C. (2014). GPU Accelerated Implementation of Density Functional Theory for Hybrid QM/MM Simulations. *Journal of Chemical Theory and Computation*, *10*(3), 959–967. https://doi.org/10.1021/ct400308n

O'Ferrall, R. A. M. (1970). Relationships between E2 and E1cB mechanisms of β-elimination. *J. Chem. Soc. B*, *0*, 274–277. https://doi.org/10.1039/J29700000274

Otten, R., Pádua, R. A. P., Bunze, H. A., Nguyen, V., Pitsawong, W., Patterson, M., Sui, S.,

Perry, S. L., Cohen, A. E., Hilvert, D., & Kern, D. (2020). How directed evolution reshapes the energy landscape in an enzyme to boost catalysis. *Science*, *370*(6523), 1442–1446. https://doi.org/10.1126/science.abd3623

Ozer, G., Quirk, S., & Hernandez, R. (2012). Thermodynamics of Decaalanine Stretching in Water Obtained by Adaptive Steered Molecular Dynamics Simulations. *Journal of Chemical Theory and Computation*, *8*(11), 4837–4844. https://doi.org/10.1021/ct300709u

Ozer, G., Valeev, E. F., Quirk, S., & Hernandez, R. (2010). Adaptive Steered Molecular Dynamics of the Long-Distance Unfolding of Neuropeptide Y. *Journal of Chemical Theory and Computation*, *6*(10), 3026–3038. https://doi.org/10.1021/ct100320g

Pabis, A., Duarte, F., & Kamerlin, S. C. L. (2016). Promiscuity in the Enzymatic Catalysis of Phosphate and Sulfate Transfer. *Biochemistry*, *55*(22), 3061–3081. https://doi.org/10.1021/acs.biochem.6b00297

Palermo, G., Cavalli, A., Klein, M. L., Alfonso-Prieto, M., Dal Peraro, M., & De Vivo, M. (2015). Catalytic metal ions and enzymatic processing of DNA and RNA. *Accounts of Chemical Research*, *48*(2), 220–228. https://doi.org/10.1021/ar500314j

Perdew, J. P., Burke, K., & Ernzerhof, M. (1996). Generalized Gradient Approximation Made Simple. *Physical Review Letters*, *77*(18), 3865–3868. https://doi.org/10.1103/PhysRevLett.77.3865

Pérez-Gallegos, A., Garcia-Viloca, M., González-Lafont, À., & Lluch, J. M. (2015). SP20 Phosphorylation Reaction Catalyzed by Protein Kinase A: QM/MM Calculations Based on Recently Determined Crystallographic Structures. *ACS Catalysis*, *5*(8), 4897–4912. https://doi.org/10.1021/acscatal.5b01064

Pérez-Gallegos, A., Garcia-Viloca, M., González-Lafont, À., & Lluch, J. M. (2017). Understanding how cAMP-dependent protein kinase can catalyze phosphoryl transfer in the presence of Ca 2+ and Sr 2+: A QM/MM study. *Physical Chemistry Chemical Physics*, *19*(16), 10377–10394. https://doi.org/10.1039/C7CP00666G

Pontiggia, F., Pachov, D. V., Clarkson, M. W., Villali, J., Hagan, M. F., Pande, V. S., &

Kern, D. (2015). Free energy landscape of activation in a signalling protein at atomic resolution. *Nature Communications*, *6*(1), 7284. https://doi.org/10.1038/ncomms8284

Quesne, M. G., Borowski, T., & de Visser, S. P. (2016). Quantum Mechanics/Molecular Mechanics Modeling of Enzymatic Processes: Caveats and Breakthroughs. *Chemistry-A European Journal*, *22*(8), 2562–2581. https://doi.org/10.1002/chem.201503802

Ramírez, C. L., Zeida, A., Jara, G. E., Roitberg, A. E., & Martí, M. A. (2014). Improving Efficiency in SMD Simulations Through a Hybrid Differential Relaxation Algorithm. *Journal of Chemical Theory and Computation*, *10*(10), 4609–4617. https://doi.org/10.1021/ct500672d

Rosta, E., Yang, W., & Hummer, G. (2014). Calcium Inhibition of Ribonuclease H1 Two-Metal Ion Catalysis. *Journal of the American Chemical Society*, *136*(8), 3137–3144. https://doi.org/10.1021/JA411408X

Roston, D., & Cui, Q. (2016). Substrate and Transition State Binding in Alkaline Phosphatase Analyzed by Computation of Oxygen Isotope Effects. *Journal of the American Chemical Society*, *138*(36), 11946–11957. https://doi.org/10.1021/jacs.6b07347

Roston, D., Lu, X., Fang, D., Demapan, D., & Cui, Q. (2018). Analysis of Phosphoryl-Transfer Enzymes with QM/MM Free Energy Simulations. In *Methods in Enzymology* (Vol. 607, pp. 53–90). Elsevier Inc. https://doi.org/10.1016/bs.mie.2018.05.005

Royer, C. A. (2008). The nature of the transition state ensemble and the mechanisms of protein folding: A review. *Archives of Biochemistry and Biophysics*, *469*(1), 34–45. https://doi.org/10.1016/j.abb.2007.08.022

Saen-Oon, S., Ghanem, M., Schramm, V. L., & Schwartz, S. D. (2008). Remote mutations and active site dynamics correlate with catalytic properties of purine nucleoside phosphorylase. *Biophysical Journal*, *94*(10), 4078–4088.

https://doi.org/10.1529/biophysj.107.121913

Schramm, V. L. (2007). Enzymatic Transition State Theory and Transition State Analogue Design. *Journal of Biological Chemistry*, *282*(39), 28297–28300. https://doi.org/10.1074/jbc.R700018200

Schramm, V. L., & Schwartz, S. D. (2018). Promoting Vibrations and the Function of Enzymes. Emerging Theoretical and Experimental Convergence. *Biochemistry*, *57*(24), 3299–3308. https://doi.org/10.1021/ACS.BIOCHEM.8B00201

Schwartz, S. D., & Schramm, V. L. (2009). Enzymatic transition states and dynamic motion in barrier crossing. *Nature Chemical Biology*, *5*(8), 551–558. https://doi.org/10.1038/nchembio.202

Seabra, G. de M., Walker, R. C., Elstner, M., Case, D. A., & Roitberg, A. E. (2007). Implementation of the SCC-DFTB Method for Hybrid QM/MM Simulations within the Amber Molecular Dynamics Package †. *The Journal of Physical Chemistry A*, *111*(26), 5655–5664. https://doi.org/10.1021/jp070071l

Senn, H. M., & Thiel, W. (2009). QM/MM methods for biomolecular systems. *Angewandte Chemie (International Ed. in English)*, *48*(7), 1198–1229. https://doi.org/10.1002/anie.200802019

Shibanuma, Y., Nemoto, N., Yamamoto, N., Sampei, G.-I., & Kawai, G. (2020). Crystal structure of adenylate kinase from an extremophilic archaeon Aeropyrum pernix with ATP and AMP. *The Journal of Biochemistry*, *168*(3), 223–229. https://doi.org/10.1093/jb/mvaa043

Stiller, J. B., Jordan Kerns, S., Hoemberger, M., Cho, Y. J., Otten, R., Hagan, M. F., & Kern, D. (2019). Probing the transition state in enzyme catalysis by high-pressure NMR dynamics. *Nature Catalysis*, *2*(8), 726–734. https://doi.org/10.1038/s41929-019-0307-6

Stiller, J. B., Otten, R., Häussinger, D., Rieder, P. S., Theobald, D. L., & Kern, D. (2022). Structure determination of high-energy states in a dynamic protein ensemble. *Nature*, *603*(7901), 528–535. https://doi.org/10.1038/s41586-022-04468-9

Stockbridge, R. B., & Wolfenden, R. (2009). The Intrinsic Reactivity of ATP and the Catalytic Proficiencies of Kinases Acting on Glucose, N-Acetylgalactosamine, and Homoserine. *Journal of Biological Chemistry*, *284*(34), 22747–22757. https://doi.org/10.1074/jbc.M109.017806

Truhlar, D. G. (2015). Transition state theory for enzyme kinetics. *Archives of Biochemistry and Biophysics*, *582*, 10–17. https://doi.org/10.1016/j.abb.2015.05.004

Tsai, C. J., & Nussinov, R. (2014). A Unified View of "How Allostery Works." *PLoS Computational Biology*, *10*(2), e1003394. https://doi.org/10.1371/journal.pcbi.1003394

Turjanski, A. G., Hummer, G., & Gutkind, J. S. (2009). How Mitogen-Activated Protein Kinases Recognize and Phosphorylate Their Targets: A QM/MM Study. *Journal of the American Chemical Society*, *131*(17), 6141–6148. https://doi.org/10.1021/ja8071995

Valiev, M., Yang, J., Adams, J. a, Taylor, S. S., & Weare, J. H. (2007). Phosphorylation reaction in cAPK protein kinase-free energy quantum mechanical/molecular mechanics simulations. *The Journal of Physical Chemistry. B*, *111*(47), 13455–13464. https://doi.org/10.1021/jp074853q

van der Kamp, M. W., & Mulholland, A. J. (2013). Combined Quantum Mechanics/Molecular Mechanics (QM/MM) Methods in Computational Enzymology. *Biochemistry*, *52*(16), 2708–2728. https://doi.org/10.1021/bi400215w

Walker, R. C., Crowley, M. F., & Case, D. A. (2008). The implementation of a fast and accurate QM/MM potential method in Amber. *Journal of Computational Chemistry*, *29*(7), 1019–1031. https://doi.org/10.1002/JCC.20857

Warshel, A., & Bora, R. P. (2016). Perspective: Defining and quantifying the role of dynamics in enzyme catalysis. *The Journal of Chemical Physics*, *144*(18), 180901. https://doi.org/10.1063/1.4947037

Westheimer, F. (1987). Why nature chose phosphates. *Science*, *235*(4793), 1173–1178. https://doi.org/10.1126/science.2434996

Wolf-Watz, M., Thai, V., Henzler-Wildman, K., Hadjipavlou, G., Eisenmesser, E. Z., & Kern, D. (2004). Linkage between dynamics and catalysis in a thermophilic-mesophilic enzyme pair. *Nature Structural and Molecular Biology*, *11*(10), 945–949. https://doi.org/10.1038/nsmb821

Yang, L., Liao, R.-Z., Ding, W.-J., Liu, K., Yu, J.-G., & Liu, R.-Z. (2012). Why calcium inhibits magnesium-dependent enzyme phosphoserine phosphatase? A theoretical study. *Theoretical Chemistry Accounts 2012 131:9*, *131*(9), 1–12. https://doi.org/10.1007/S00214-012-1275-Y

Yang, Y., Yu, H., York, D., Elstner, M., & Cui, Q. (2008). Description of Phosphate Hydrolysis Reactions with the Self-Consistent-Charge Density-Functional-Tight-Binding (SCC-DFTB) Theory. 1. Parameterization. *Journal of Chemical Theory and Computation*, *4*(12), 2067–2084. https://doi.org/10.1021/ct800330d

Zinovjev, K., & Tuñón, I. (2017). Quantifying the limits of transition state theory in enzymatic catalysis. *Proceedings of the National Academy of Sciences*, *114*(47), 12390–12395. https://doi.org/10.1073/pnas.1710820114

468

Figures

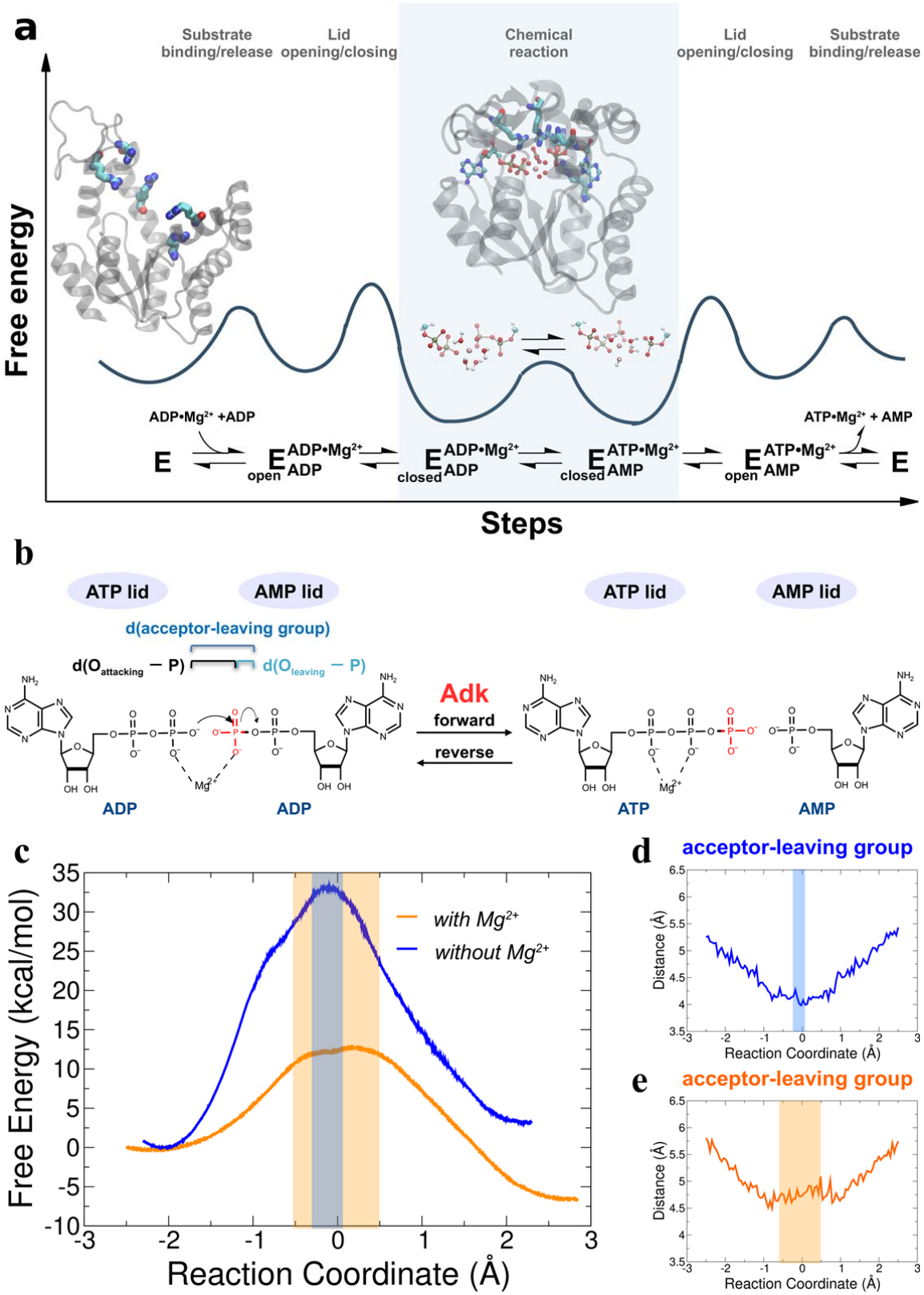

Figure 1: Investigation of the chemical step of phosphoryl transfer by QM/MM calculations in the enzymatic reaction of Adk. a) Complete reaction scheme with correspond-

ing illustrative free-energy landscape highlighting the chemical phosphoryl-transfer step (modified from ref. (Kerns et al., 2015)). Protein structures shown are apo Adk in the open conformation and Adk in the closed conformation with two bound ADP molecules and one Mg^{2+} atom (active-site arginine side chains are shown in stick representation). **b)** Phosphoryl-transfer step is drawn with corresponding distances used to define the reaction coordinate as used in panels d,e. **c)** Free-energy profiles for the Adk catalyzed interconversion of ADP-ADP into ATP-AMP in the absence (blue) and presence of Mg^{2+} (orange) from QM/MM calculations. AD(T)P is fully charged for the reaction with Mg^{2+}, and singly protonated on one ADP β-oxygen for reaction without Mg^{2+}. The reaction coordinate is defined as the difference between the distance of the leaving oxygen to the transferring phosphorus $d(O_{leaving}\text{-}P)$ and the distance of the attacking oxygen to the transferring phosphorus $d(O_{attacking}\text{-}P)$. **d,e)** Distance between acceptor and leaving oxygens along the reaction coordinate in the presence (e) and in the absence (d) of Mg^{2+}. The transition state regions in c-e are highlighted in orange and grey, respectively.

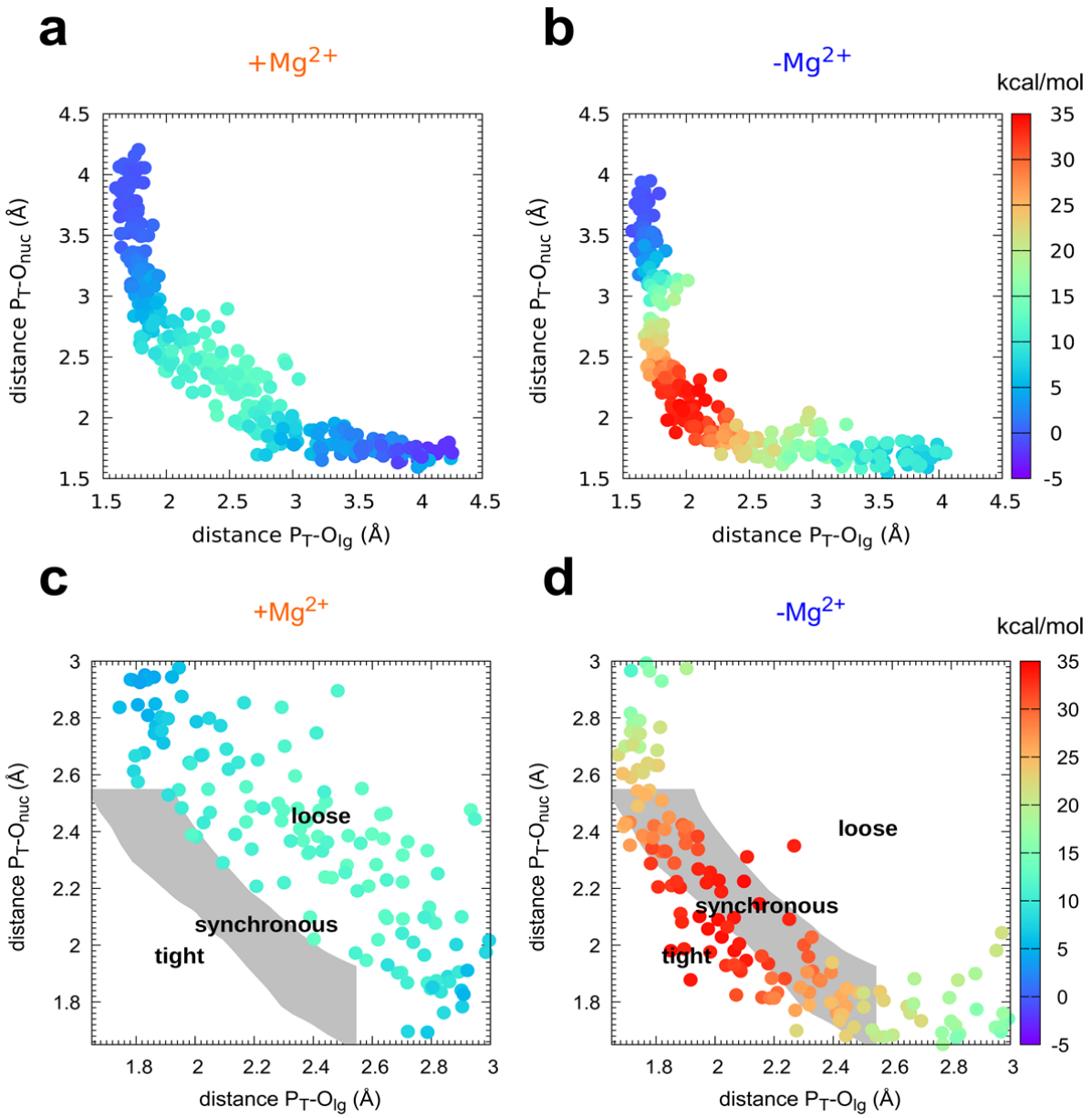

493 **Figure 2**: **Mechanism of phosphoryl transfer.** Diagram of Moore-O'Ferrall-Jencks
494 (Jencks, 2002; O'Ferrall, 1970) from the QM/MM simulations, plotting the two P-O
495 distances involved in the P-transfer for the reaction **a,c)** with Mg^{2+} and **b,d)** without Mg^{2+}
496 (P_T for transferring phosphate). The theoretical transition pathways for a tight, synchronous,
497 and loose transition state are shown in c,d (as defined in ref. Roston et al. (Roston & Cui,
498 2016)).

499

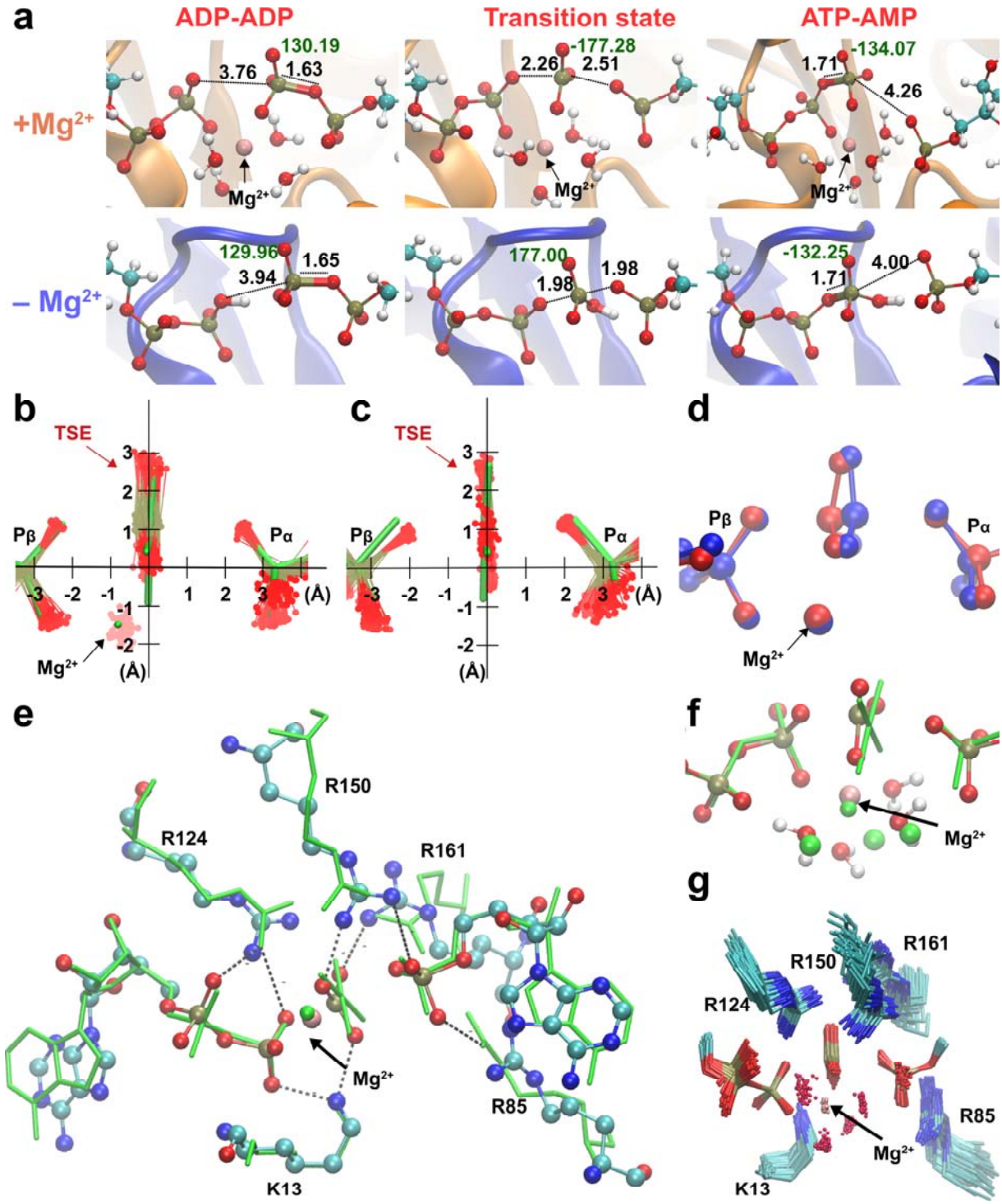
a
ADP-ADP
Transition state
ATP-AMP
+Mg2+
– Mg2+
130.19
3.76
1.63
Mg2+
-177.28
2.26
2.51
Mg2+
-134.07
1.71
4.26
Mg2+
129.96
3.94
1.65
177.00
1.98
1.98
-132.25
1.71
4.00
b
TSE
Pβ
Pα
Mg2+
(Å)
c
TSE
Pβ
Pα
(Å)
d
Pβ
Pα
Mg2+
e
R150
R124
R161
Mg2+
R85
K13
f
Mg2+
g
R161
R150
R124
R85
Mg2+
K13

Figure 3: Broad transition-state ensemble (TSE) in fully active enzyme. a) Representative snapshots for structure of reactants, transition states, and products in the Adk active site in the presence and absence of magnesium. d($O_{attacking}$-P) and d($O_{leaving}$-P) are shown. Labels in black indicate the length of the bonds involved in the phosphate transfer and in green, the dihedral angle of the phosphoryl group. **b,c)** Superposition of the transition-state ensembles reveals a wider TSE with Mg^{2+} (b) relative to the one without the cation (c) with mean rmsd (± s.d.) of distances of the central P atom from its "average" position of 0.30 ± 0.11 Å (b) and 0.13 ± 0.06 Å (c). The TSE's are superimposed with the X-ray structure solved with a transition-state analogue in green (AMP, AlF_4^- and ADP) reported in ref. (Kerns et al., 2015) (PDBID: 3SR0). **d)** Superposition of two extreme structures out of the large TSE for the enzyme with Mg^{2+}, one where the phosphoryl group is closest to the donor oxygen (blue) and the other closest to the acceptor oxygen (red) highlighting the asymmetric character of TSE members. **e, f)** superposition of most symmetric snapshot from TSE of QM/MM calculations (ball and stick representation in cyan) with the X-ray structure of transition-state analogue (green, PDBID: 3SR0 (Kerns et al., 2015)) including coordinating water molecules in f). **g)** zoom into the active site to display the broad TSE in the presence of Mg^{2+} aided by flexible Arg and Lys side chains in the active site.

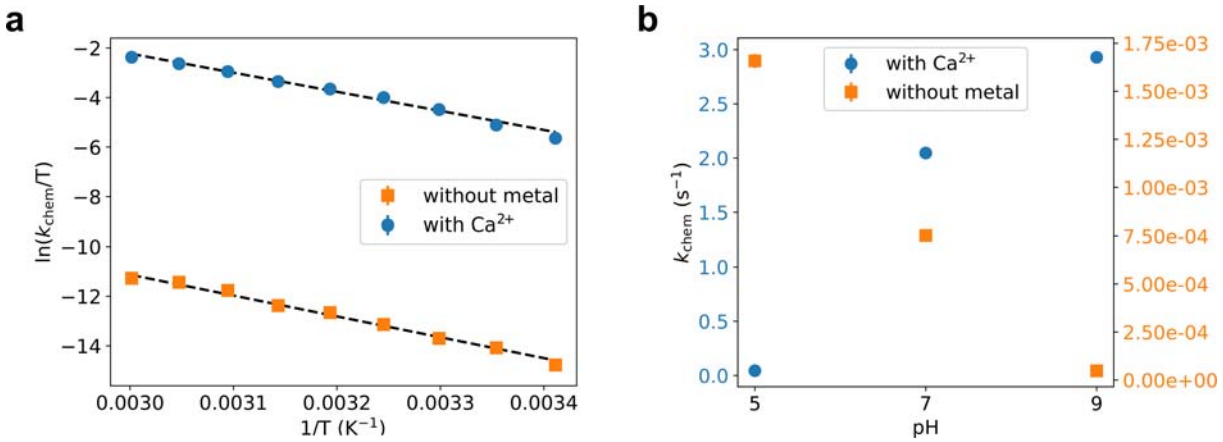

521 **Figure 4: Experimental testing of the computational findings. a,b)** Turnover rate
522 constants that represent the chemical step (k_{chem}) under these conditions were measured
523 with 8 mM ADP/Mg^{2+} by HPLC detection of build-up of ATP and AMP. **a)** Temperature
524 dependence of the phosphoryl transfer step measured in presence of calcium and in
525 absence of divalent any cations, plotted as Eyring plots. Fits to the Eyring equation
526 (dashed lines) result in $\Delta H^{\ddagger}$ = 70.0 ± 4.1 kJ mol^{-1} and $\Delta S^{\ddagger}$ = -80.0 ± 12.8 J mol-1 K^{-1}
527 without metal, and $\Delta H^{\ddagger}$ = 64.1 ± 2.2 kJ mol^{-1} and $\Delta S^{\ddagger}$ = -23.8 ± 6.8 J mol^{-1} K^{-1} with Ca^{2+}. **b)**
528 pH dependence of k_{chem} measured in the presence of calcium and in absence of any
529 divalent cation.

530 **Tables**

531

532 **Table 1. Free-energy profile estimates of the free-energy parameters of the reaction,**
533 **using SCC-DFTB (all values in kcal/mol).** ΔG^o: Overall reaction free-energy; $\Delta_f G^{\ddagger}$:
534 Activation free-energy of the forward reaction. $\Delta_b G^{\ddagger}$: Activation free-energy of the
535 backward reaction. ξ(TS) is the range of the reaction coordinate in the TSE (in Å); *ζ*(TS) is
536 the improper dihedral angle of the transferring phosphate in the TS. The estimated errors
537 of the free energies are in parenthesis and are computed as described in materials and
538 methods.

539

	with Mg^{2+}	without Mg^{2+}	with Mg^{2+}, ADP monoprotonated
ΔG^o	-6 (1.7)	+4 (2.5)	+6 (1.9)
$\Delta_f G^{\ddagger}$	13 (0.9)	34 (1.6)	23 (0.9)
$\Delta_b G^{\ddagger}$	20 (0.8)	30 (0.9)	18 (0.9)
ξ(TS)	-0.5－0.7	-0.2－0	-0.3－-0.1
ζ(TS)	160－200	165-180	170-180

540

541

542

543 **Table 2. Experimentally determined observed rate constants of the forward and**
544 **backward chemical reactions for mutant forms of Adk in the presence of Mg^{2+}.** Note
545 that the corresponding rate constants for the phosphoryl transfer in the wild-type protein
546 are too fast to be directly measured and have been estimated to be more than three orders
547 of magnitude faster than in the mutants (Kerns et al., 2015).

548

AAdk mutant	rate constant (s^{-1}) 2 ADP → ATP + AMP	rate constant (s^{-1}) ATP + AMP → 2 ADP
R124K	4.6 ± 0.5	1.6 ± 0.4
R150K	1.3 ± 0.3	1.1 ± 0.3
R161K	0.4 ± 0.1	0.5 ± 0.2
R85K	0.3 ± 0.1	1.6 ± 0.2
R36K	0.8 ± 0.2	14 ± 2

549

550

551

552 **Supplementary Figures**

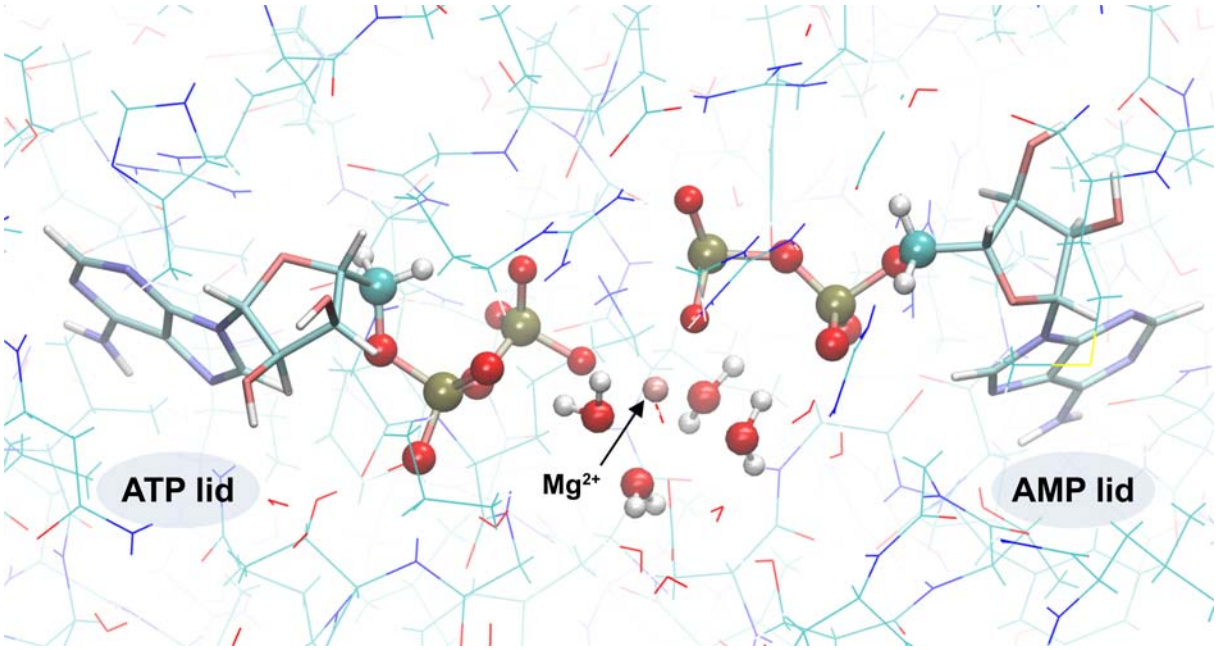

553 **Figure 1 – supplement 1. QM/MM system.** The QM subsystem is shown in CPK repre-
554 sentation and the MM subsystem is in lines representation.
555
556
557
558

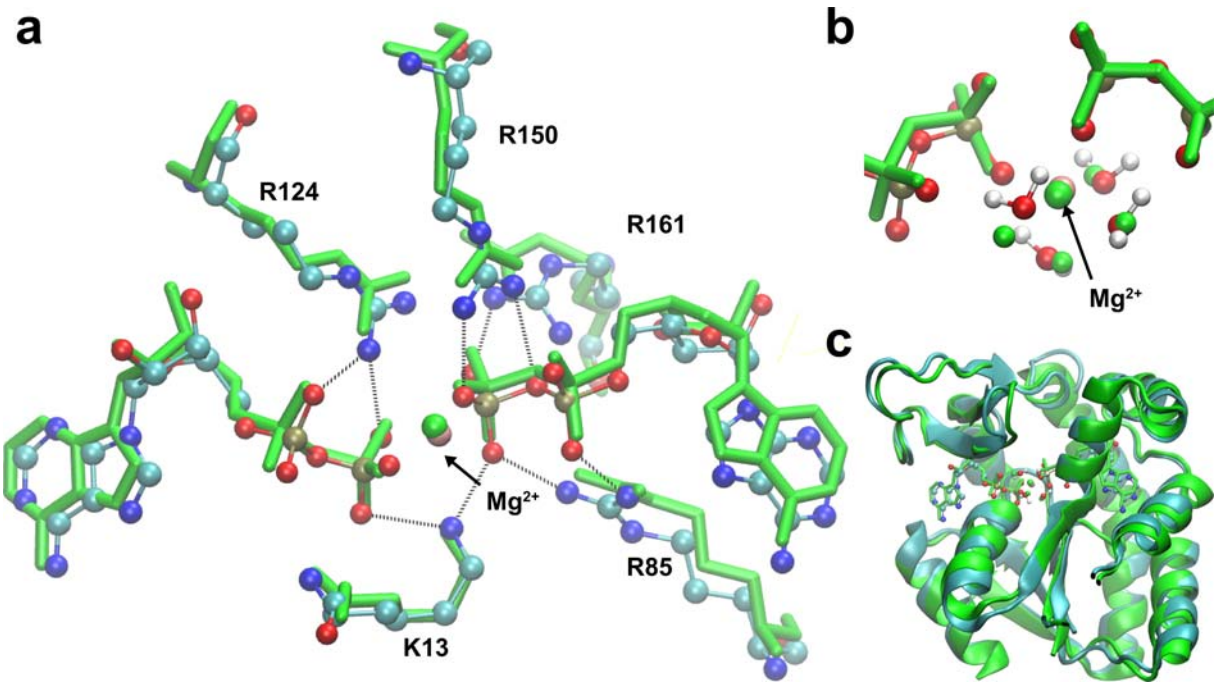

559 **Figure 1 – supplement 2. Superposition of the starting model structure for QM/MM**
560 **and the crystallographic structure (PDB ID: 4CF7 (Kerns et al., 2015)) of Adk with 2**
561 **ADP/Mg bound**. **a)** Comparison of ADPs, main amino acids and Mg^{2+} ion in the active site
562 against the crystallographic model in green (starting structure for QM/MM as ball and
563 stick), **b)** zoom-in showing Mg^{2+} ion coordinated by water molecules and the phosphates,
564 and **c)** the Adk backbone of the starting model (cyan) and the crystallographic structure
565 (green) with a backbone RMSD of 0.98 Å.

566

567

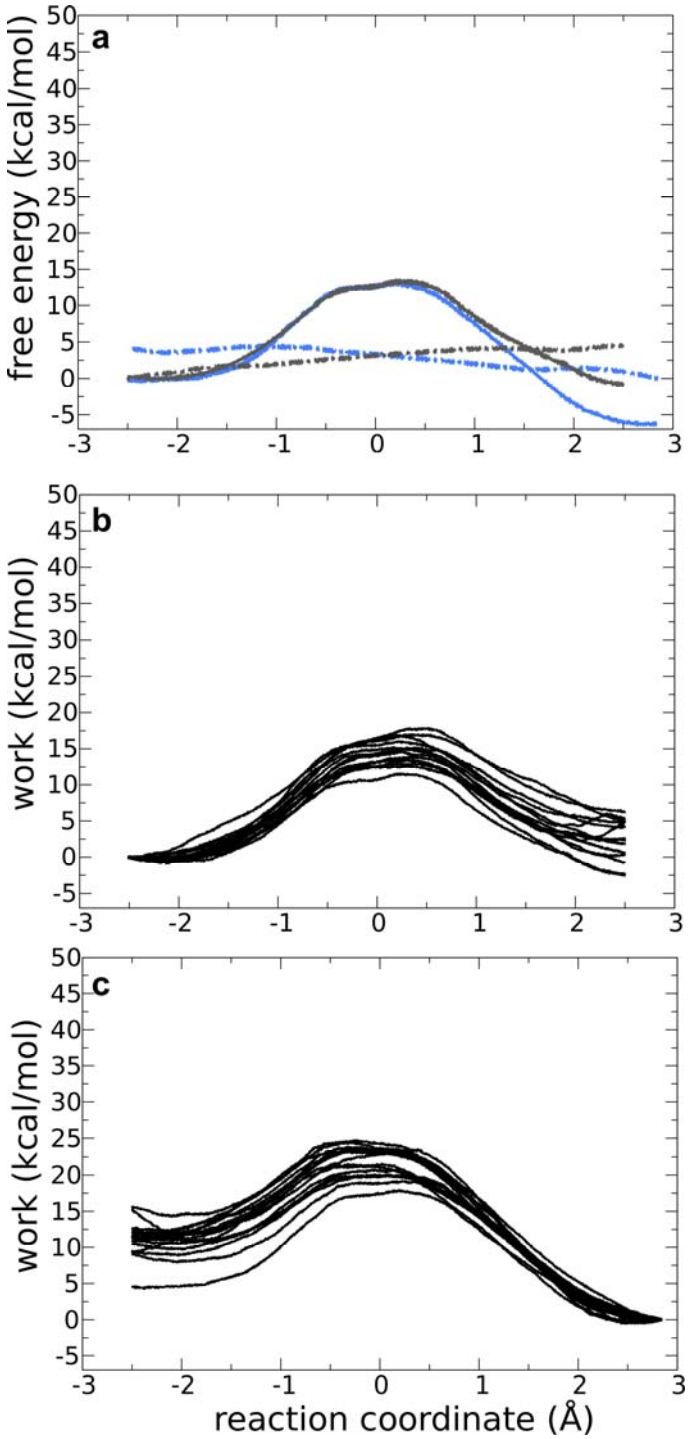

568

569 **Figure 1 – supplement 3. Forward and backward QM/MM reactions for Adk with two**
570 **ADP and Mg^{2+} bound a)** Free energy profile (FEP) for the forward (solid grey line) and
571 backward (solid blue line) reactions for the *nonprotonated system in the presence of Mg^{2+}*.
572 The dashed lines are the standard deviation for the forward and backward reactions in

grey and blue, respectively. **b,c)** Works profiles obtained for the forward (b) and backward (c) reaction.

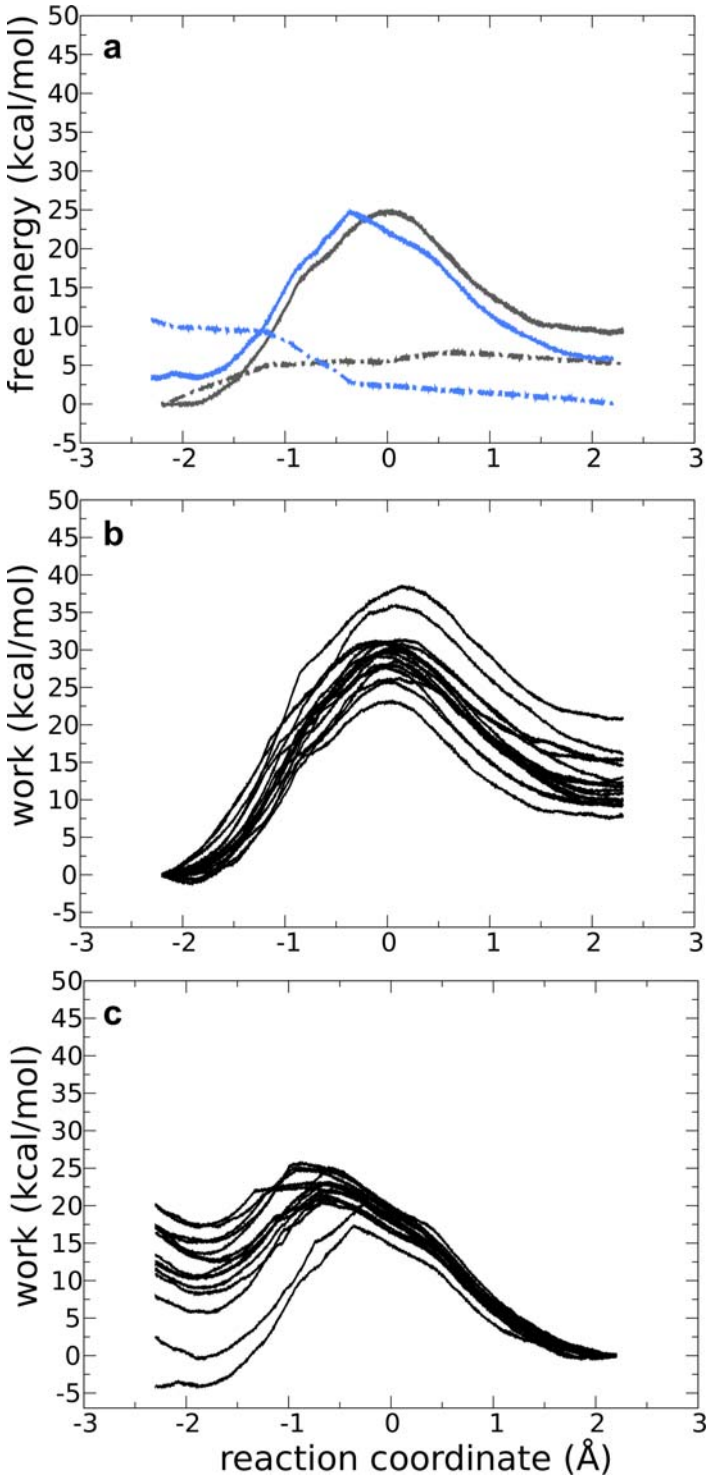

577 **Figure 1 – supplement 4. Forward and backward QM/MM reactions for Adk with**
578 **ADP, ADP and Mg^{2+} bound a)** Free energy profile for the forward (solid grey line) and
579 backward (solid blue line) reactions for the *monoprotonated system with* Mg^{2+}. The dashed
580 lines are the standard deviation for the forward and backward reactions in grey and blue,
581 respectively. **b,c)** Works profiles obtained for the forward (b) and backward (c) reaction.

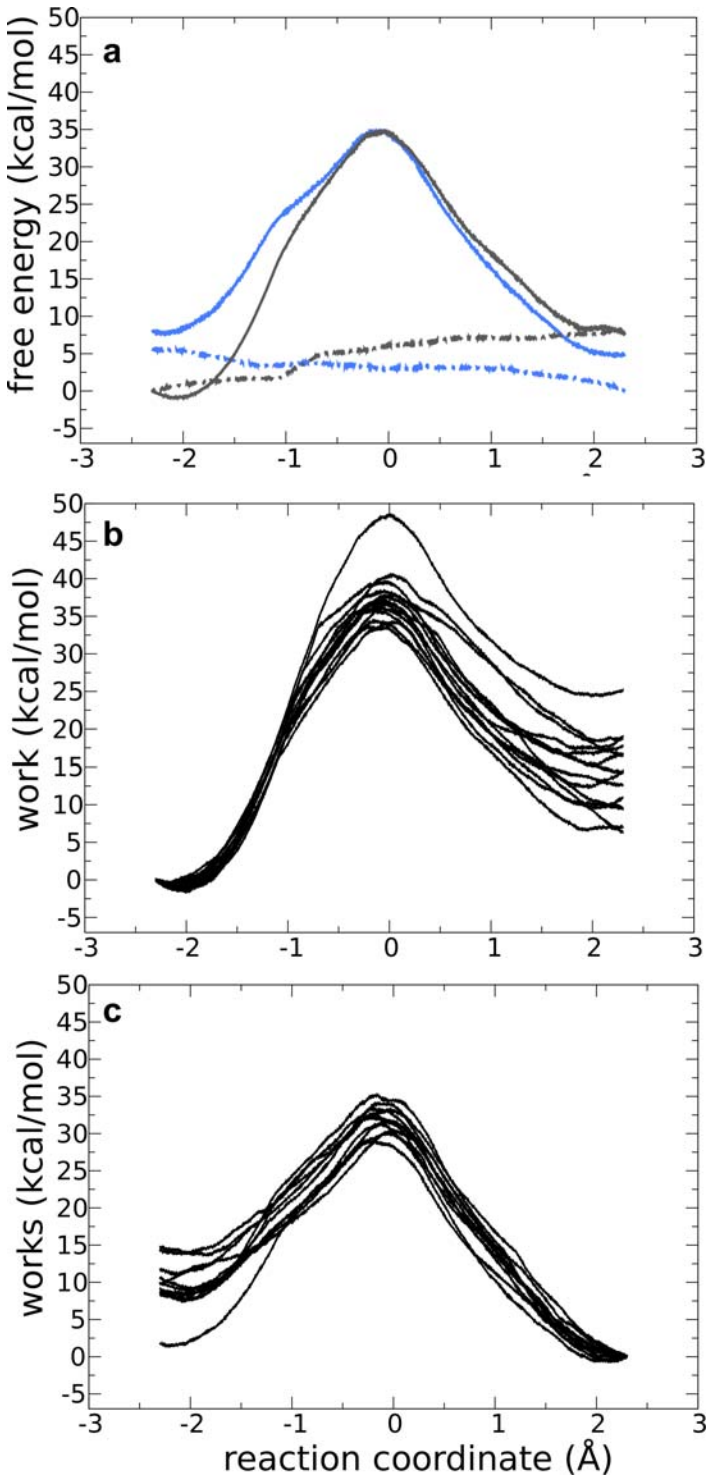

582

583 **Figure 1 – supplement 5. Forward and backward QM/MM reactions for Adk with two**
584 **ADP and without Mg^{2+} bound a)** Free energy profile for the forward (solid grey line) and
585 backward (solid blue line) reactions for the *monoprotonated system without* Mg^{2+}. The
586 dashed lines are the standard deviation for the forward and backward reactions in grey

587 and blue, respectively. **b,c)** Works profiles obtained for the forward (b) and backward (c)
588 reaction.

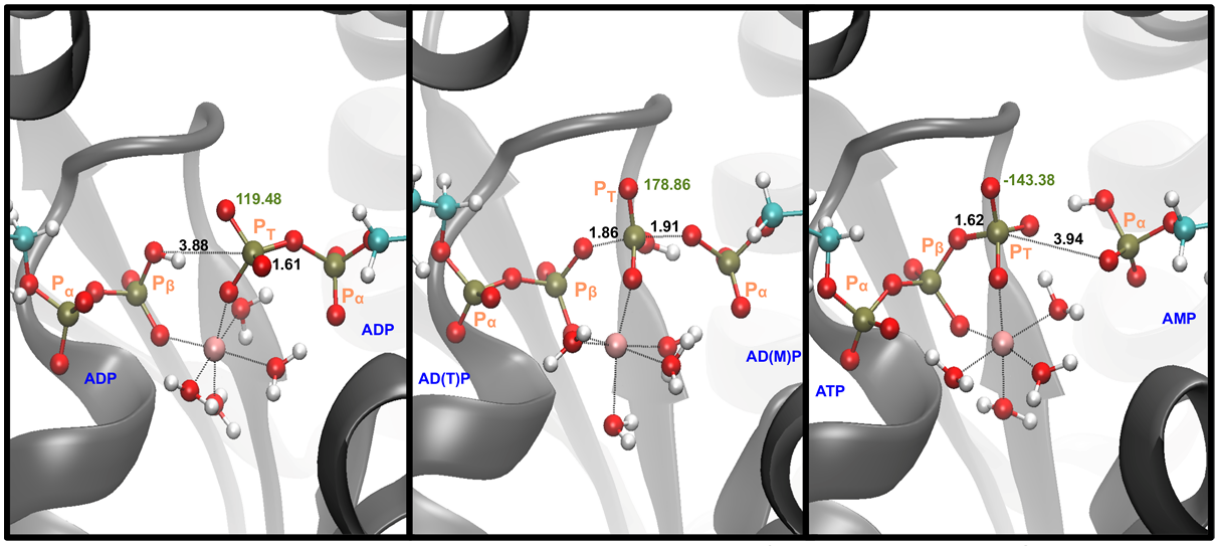

589 **Figure 3 – supplement 1.** Representative snapshots for the reactant, TS and product
590 states in the *monoprotonated system with* Mg^{2+}*.* The labels in black describe the distances
591 that are part of the phosphate transfer and the label in green show the dihedral angle.
592 Label of the phosphates in orange.

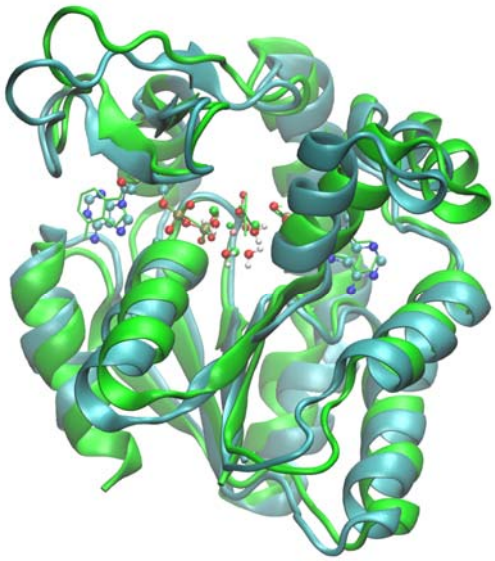

593 **Figure 3 – supplement 2. A representative transition state structure is compared**
594 **against the x-ray structure PDB ID: 3SR0 (Kerns et al., 2015).** The superposition is
595 showed for: the main active site's residues the atoms taking part of the reaction and

backbone of the Adk.

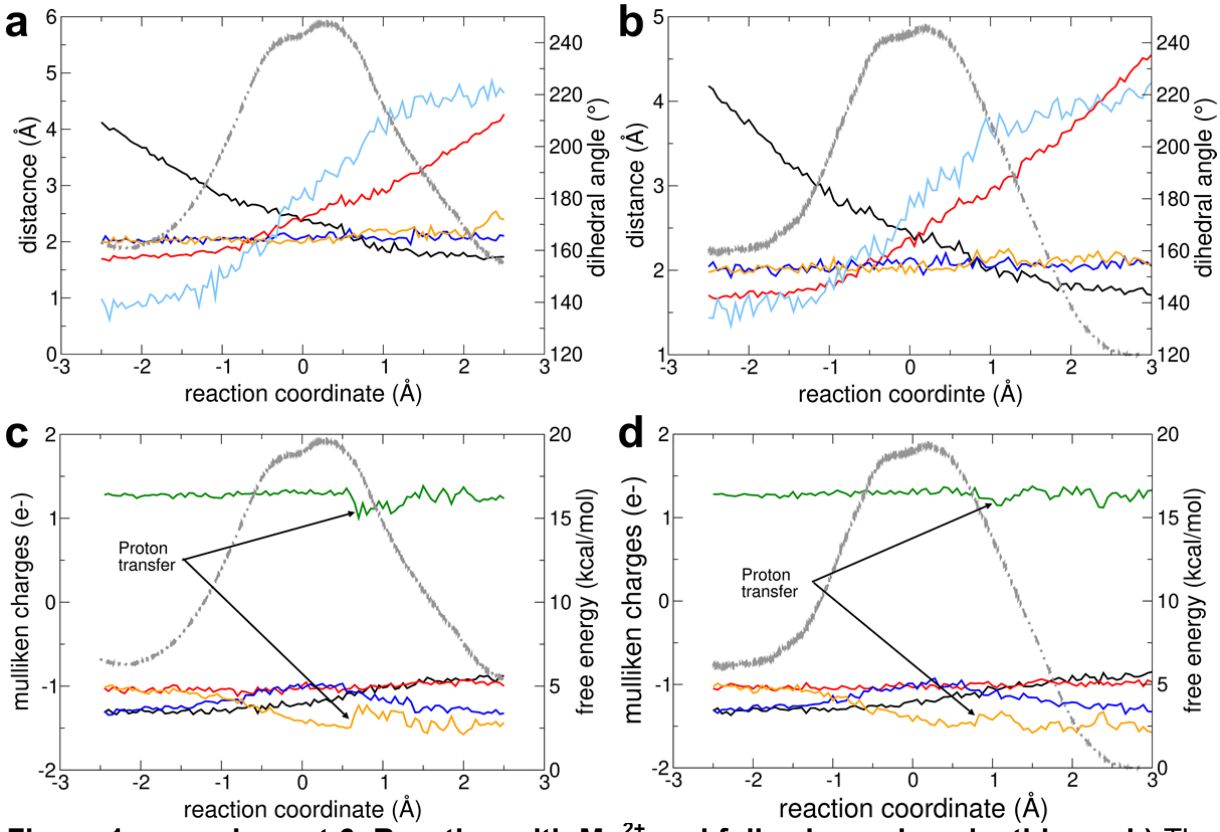

Figure 1 – supplement 6. Reaction with Mg^{2+} and fully charged nucleotides. a-b) The change in geometrical parameters along the reaction coordinate are shown for (a) forward and (b) backward reaction. Parameters: distance $O_{leaving}$ – $P_{transferring}$ (red), distance $O_{attacking}$ – $P_{transferring}$ (black), transferring phosphate dihedral angle (light blue), distance Mg^{2+} – O from transferring phosphate (blue), and distance Mg^{2+} – O from beta-phosphate of $ADP_{ATP\text{-}lid}$ (orange). **c, d)** The charge (mulliken charge) variation of different moieties involved in the reaction are shown for (c) forward and (d) backward reaction: Mg^{2+} (green), alpha-phosphate of $ADP_{ATP\text{-}lid}$ (red), alpha-phosphate of $ADP_{AMP\text{-}lid}$ (orange), beta phosphate of $ADP_{ATP\text{-}lid}$ (black), transferring phosphate (blue). Note that a proton is transiently transferred from one water molecule coordinating the Mg^{2+} to an oxygen of Pα in $ADP_{AMP\ lid}$ (leaving group). In all plots, the FEP is shown in the background as light grey dashed line.

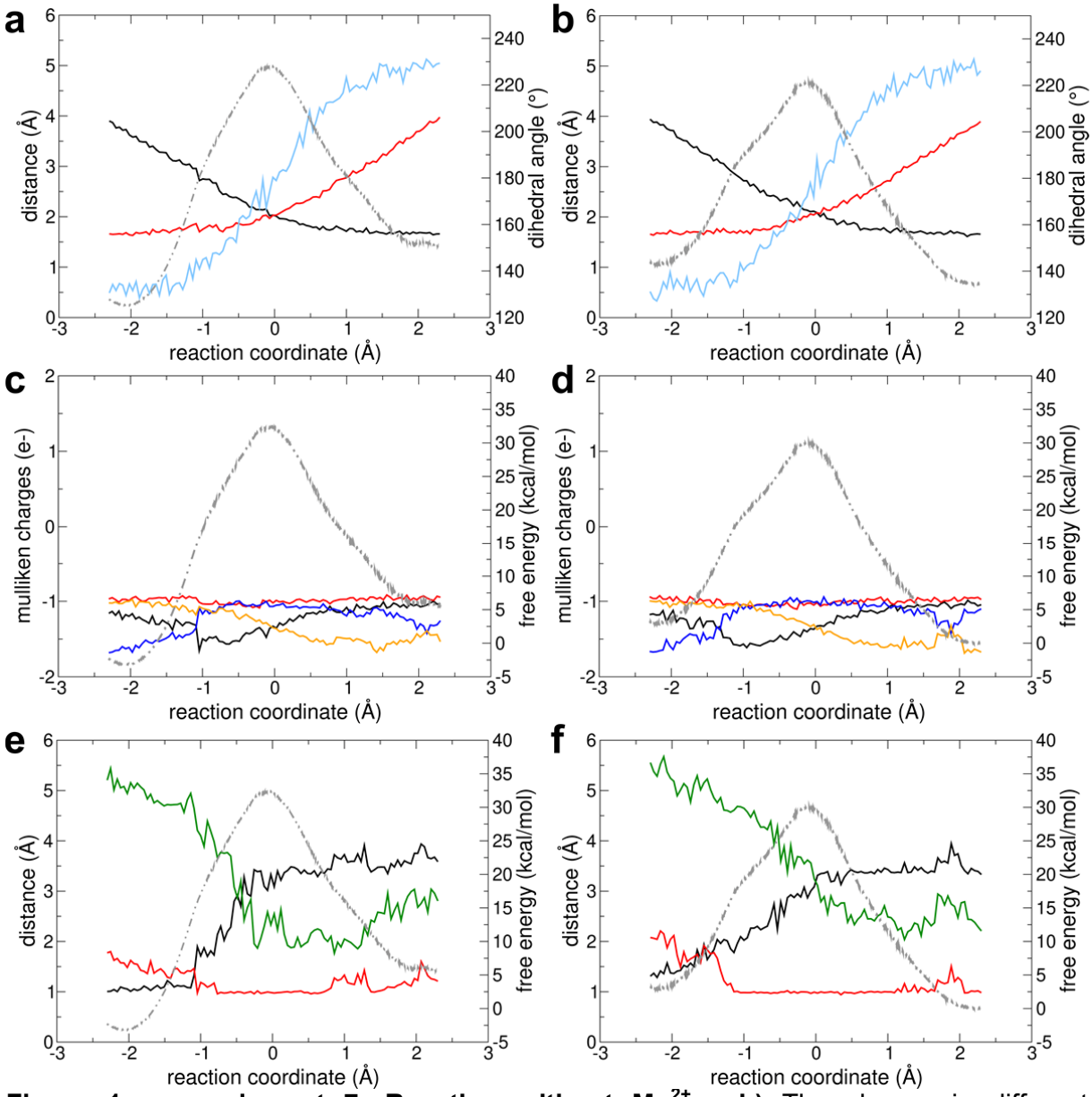

Figure 1 – supplement 7. Reaction without Mg^{2+}. a,b) The change in different geometrical parameters along the reaction coordinate are shown for (a) forward and (b) backward reaction. Parameters shown: distance $O_{leaving}$ – $P_{transferring}$ (red), distance $O_{attacking}$ – $P_{transferring}$ (black), transferring phosphate dihedral angle (light blue). **c,d)** The charge

621 (mulliken charge) variation of different moieties involved in the reaction are shown for (c)
622 forward and (d) backward reaction: alpha phosphate of $ADP_{ATP\text{-}lid}$ (red), alpha phosphate
623 of $ADP_{AMP\text{-}lid}$ (orange), beta phosphate of $ADP_{ATP\text{-}lid}$ (black), transferring phosphate (blue).
624 **e,f)** The distances involving the proton transfer are shown for (e) forward and (f) backward
625 reaction: H – $O_{attacking}$ (black), H – O of transferring phosphate (red) and H – O of alpha
626 phosphate of $ADP_{AMP\text{-}lid}$ (green). In all plots, the FEP is shown in the background as light
627 grey dashed line.

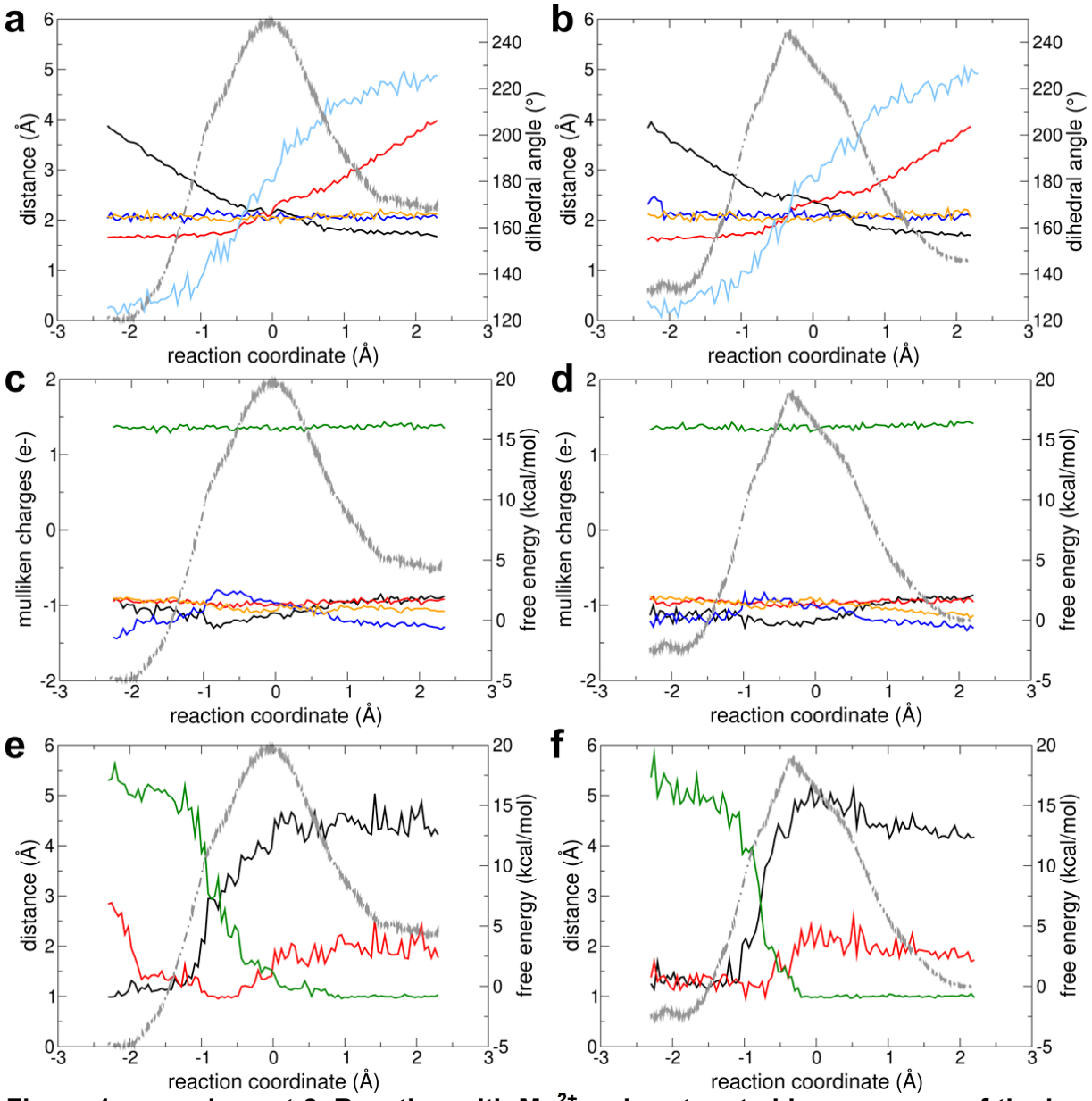

Figure 1 – supplement 8. Reaction with Mg^{2+} and protonated in an oxygen of the beta phosphate of $ADP_{ATP\text{-}lid}$. a,b) The change in different geometrical parameters along the reaction coordinate are shown for (a) forward and (b) backward reaction. Parameters shown: distance $O_{leaving} – P_{transferring}$ (red), distance $O_{attacking} – P_{transferring}$ (black), transferring phosphate dihedral angle (light blue), distance Mg^{2+} – O from transferring phosphate (blue), and distance Mg – O from beta phosphate of $ADP_{ATP\text{-}lid}$ (orange). **c,d)** The charge (mulliken charge) variation of different moieties involved in the reaction with $Mg^{2+}$are shown for (c) forward and (d) backward reaction: Mg^{2+} (green), alpha phosphate of $ADP_{ATP\text{-}lid}$ (red), alpha phosphate of $ADP_{AMP\text{-}lid}$ (orange), beta phosphate of $ADP_{ATP\text{-}lid}$ (black), transferring phosphate (blue). **e,f)** The distances involving the proton transfer are shown

for (e) forward and (f) backward reaction: H – $O_{attacking}$ (black), H – O of transferring phosphate (red) and H – O of alpha phosphate of $ADP_{AMP\text{-}lid}$ (green). In all plots, the FEP is shown in the background as light grey dashed line.

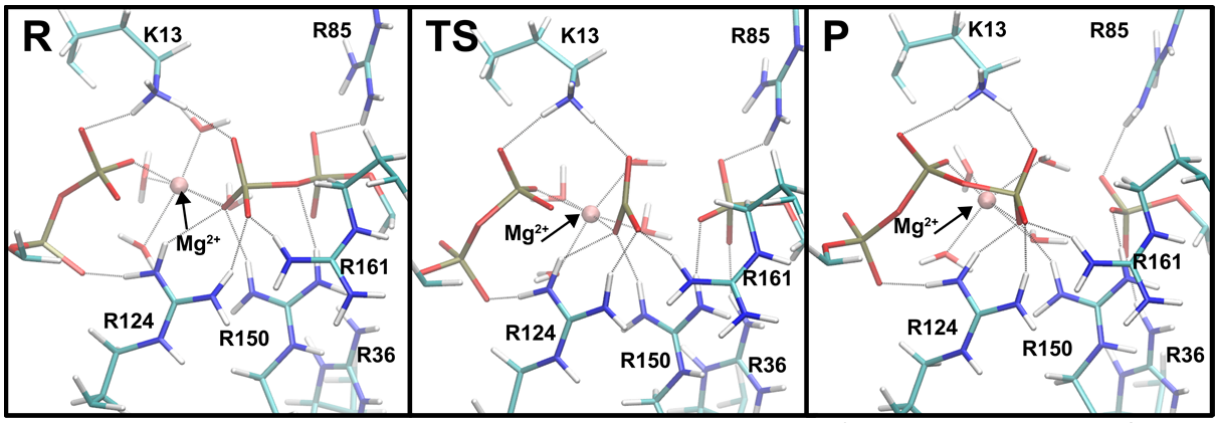

Figure 3 – supplement 3. Representative snapshots for the reactant, TS and product states in the system with Mg^{2+}. The main interactions between the phosphate moieties of the nucleotides and the amino acid side-chains in the active site are shown (in gray dashed lines).

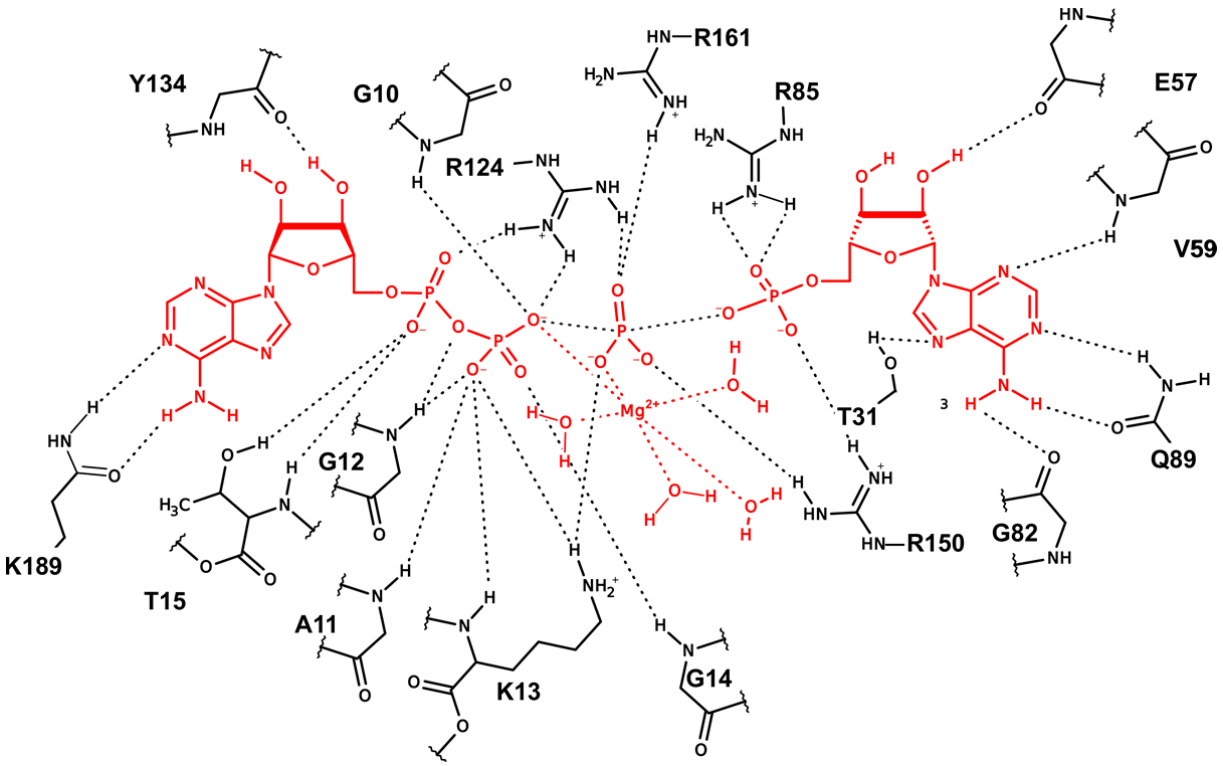

648 **Figure 3 – supplement 4.** Representation of the interactions between the nucleotides
649 with the active-site amino acids and Mg^{2+} in the active site of Adk for a representative
650 snapshot from the TSE.

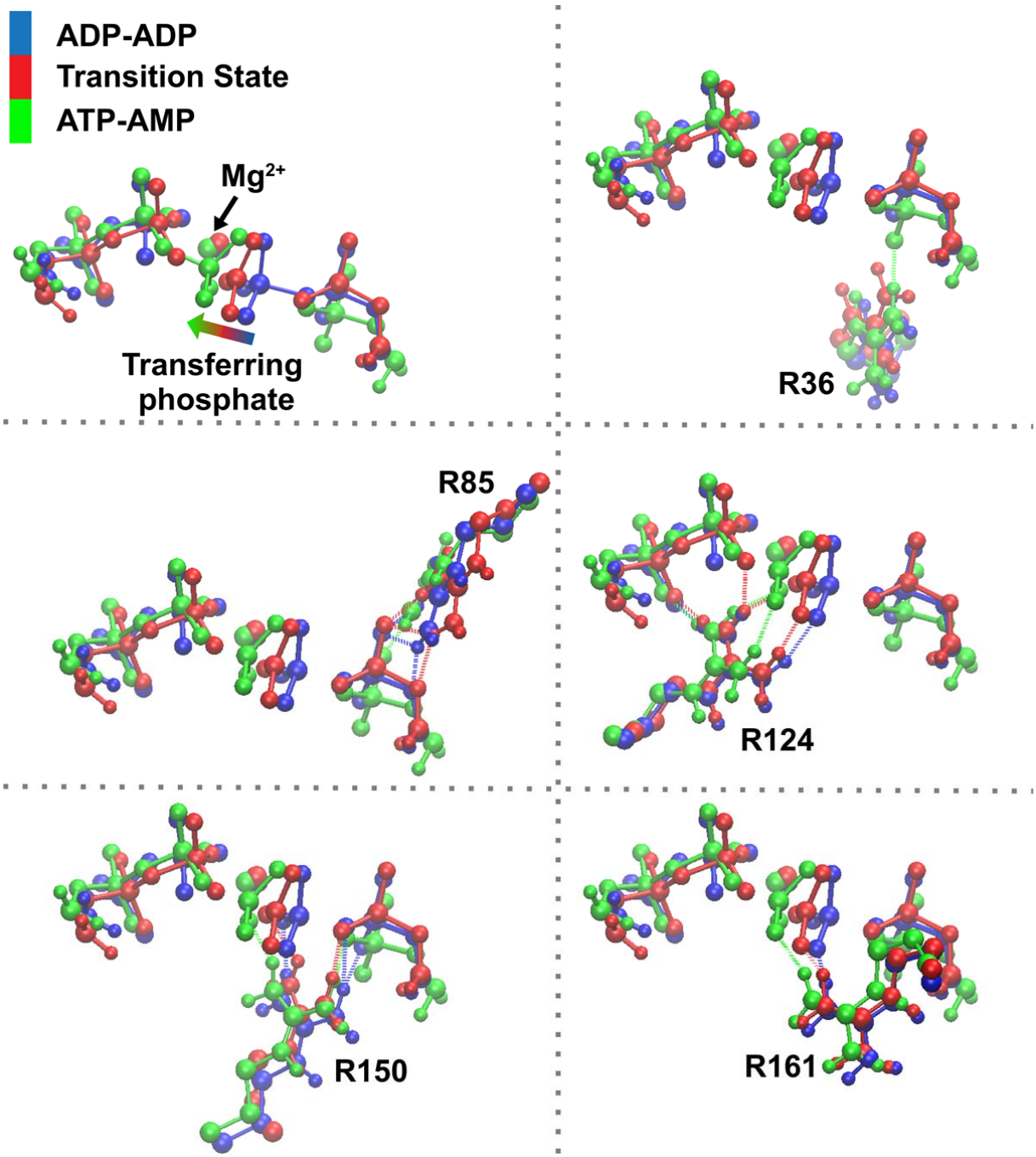

651 **Figure 3 – supplement 5.** Superposition of reactant (blue), TS (red), and product (green)
652 states focusing on the transferring phosphate and the main amino acids assisting phos-
653 phoryl transfer, for the system with Mg^{2+}.
654

655

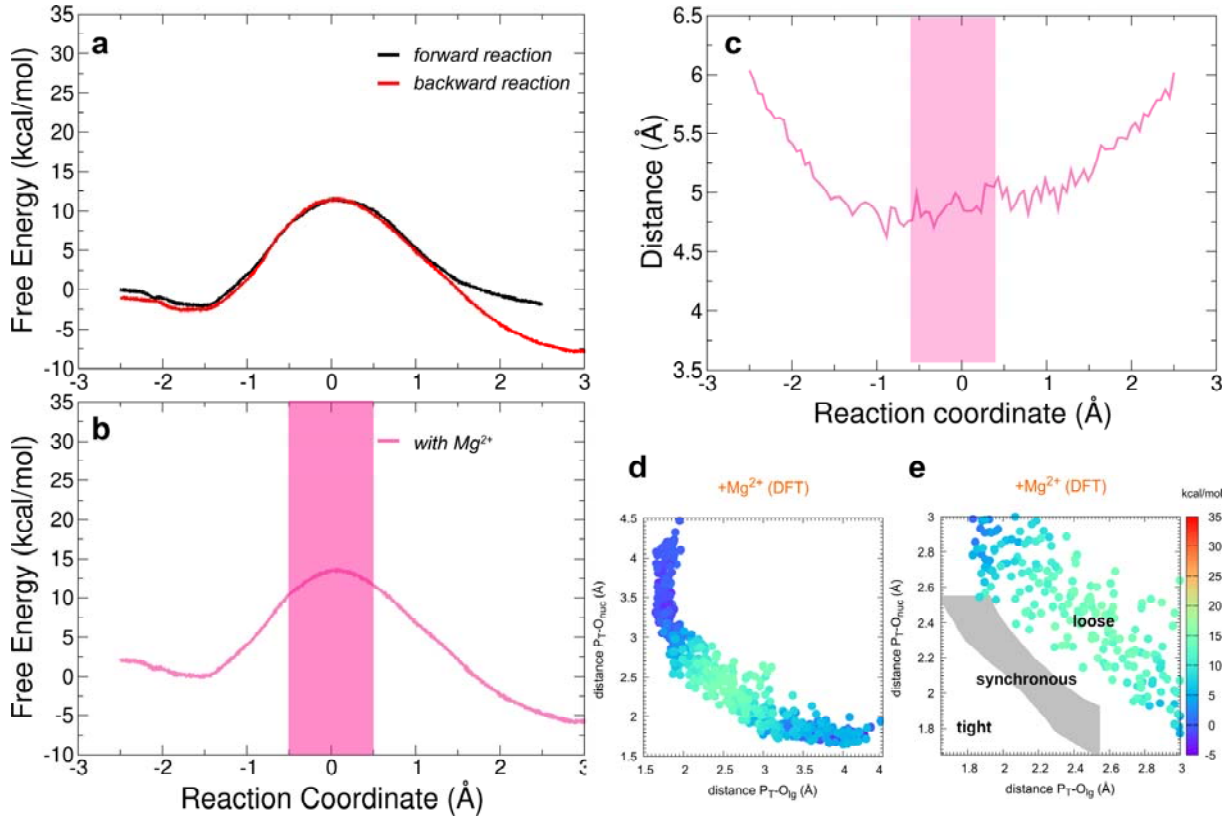

Figure 1 – supplement 9. Free-energy profiles for the Adk catalyzed interconversion of ADP-ADP into ATP-AMP and presence of Mg^{2+} employing higher level DFT(PBE) free energy calculations (see methods for details). Reaction coordinate is the same as in Fig. 1. a) Superposition of the forward and backward free-energy profiles. b) The free-energy profile as result of the combination of the forward and backward free-energy profiles. The transparent pink region shows the transition state region. c) Distance between acceptor and leaving oxygens along the reaction coordinate in the presence of Mg^{2+}. The transition state region is highlighted in pink. d,e) Diagram of Moore-O'Ferrall-Jencks (Jencks, 2002; O'Ferrall, 1970) from the simulations, plotting the two P-O distances involved in the P-transfer for the reaction with Mg^{2+}, using DFT level at the QM region (P_T for transferring

phosphate). The theoretical transition pathways for a tight, synchronous, and loose transition state are shown in e (as defined in ref. Roston et al.(Roston & Cui, 2016)).